

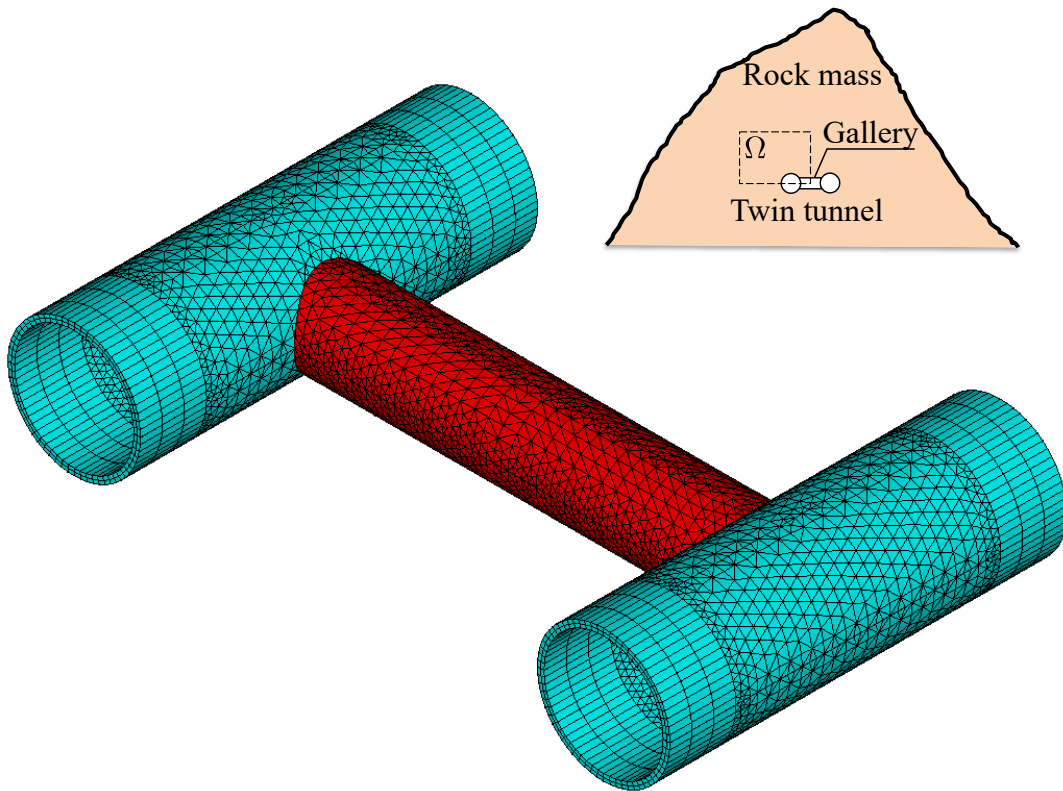
International Journal of Rock Mechanics and Mining Sciences
Numerical analysis of the rock deformation in twin tunnels with transverse galleries
considering plasticity and time-dependent constitutive models
--Manuscript Draft--

Manuscript Number:	IJRMMS-D-23-01075
Article Type:	Research paper
Keywords:	twin tunnels; transverse gallery; elastoplasticity-viscoplasticity coupling; viscoelastic lining; finite element method
Abstract:	<p>Resorting a three-dimensional finite element analysis, this paper investigates the instantaneous and long-term implications induced by the time-dependent constitutive behavior of constituents on the convergence profile of twin tunnels linked with transverse galleries. Several constitutive models for rock mass mechanical behavior are examined at the material level, encompassing elastoplasticity, viscoplasticity, or coupled elastoplasticity-viscoplasticity frameworks. Plasticity state equations are based on a Drucker-Prager yield surface with an associated flow rule, while the viscoplasticity formulation relies on the Perzyna model with a Drucker-Prager flow surface. Tunnel lining behavior is modeled using either elastic or viscoelastic constitutive models. The viscoelastic behavior is described by a Generalized Kelvin rheological model based on Bazant and Prassanann's Solidification Theory, with model parameters derived from CEB-FIP MC90 formulations. From a computational viewpoint, the deactivation-activation method is employed to simulate the excavation process and lining installation. The accuracy of finite element predictions is assessed through comparisons with available analytical solutions formulated in a simplified setting for the twin tunnels' configuration. A parametric study delves into the mutual interaction induced by tunnels proximity, emphasizing the crucial role of concrete lining stiffness in twin tunnels' deformation. Numerical simulations indicate a highly localized influence of a transverse gallery on twin tunnels deformation, extending up to four radii from each side of the gallery axis. Finally, the paper investigates the effects of twin tunnels proximity and those induced by an interconnecting gallery on the instantaneous and long-term convergence of tunnels, contrasting these outcomes with the convergence of a single tunnel.</p>

Graphical Abstract

Numerical analysis of the rock deformation in twin tunnels with transverse galleries considering plasticity and time-dependent constitutive models

Quevedo, F. P. M., Colombo, C. A. M. M., Bernaud, D., Maghous, S.



Highlights

Numerical analysis of the rock deformation in twin tunnels with transverse galleries considering plasticity and time-dependent constitutive models

Quevedo, F. P. M., Colombo, C. A. M. M., Bernaud, D., Maghous, S.

- The stiffness of the lining restricting viscous effects in the interaction of tunnels
- Interaction between the tunnels becomes significant at a span distance of 4 radii
- The viscous of the concrete lining can be important in the tunnel convergence
- The effect of the gallery extends into the tunnel up to 4 radii from its axis
- The proximity of the tunnels induces the ovalization of the tunnel wall

Numerical analysis of the rock deformation in twin tunnels with transverse galleries considering plasticity and time-dependent constitutive models

Quevedo, F. P. M.^{a,*}, Colombo, C. A. M. M.^a, Bernaud, D.^a and Maghous, S.^a

^aFederal University of Rio Grande do Sul, Av. Osvaldo Aranha, 99, Porto Alegre, 90.035-190, RS, Brazil

ARTICLE INFO

Keywords:

twin tunnels
transverse gallery
elastoplasticity-viscoplasticity coupling
viscoelastic lining
finite element method

ABSTRACT

Resorting a three-dimensional finite element analysis, this paper investigates the instantaneous and long-term implications induced by the time-dependent constitutive behavior of constituents on the convergence profile of twin tunnels linked with transverse galleries. Several constitutive models for rock mass mechanical behavior are examined at the material level, encompassing elastoplasticity, viscoplasticity, or coupled elastoplasticity-viscoplasticity frameworks. Plasticity state equations are based on a Drucker-Prager yield surface with an associated flow rule, while the viscoplasticity formulation relies on the Perzyna model with a Drucker-Prager flow surface. Tunnel lining behavior is modeled using either elastic or viscoelastic constitutive models. The viscoelastic behavior is described by a Generalized Kelvin rheological model based on Bazant and Prasanann's Solidification Theory, with model parameters derived from CEB-FIP MC90 formulations. From a computational viewpoint, the deactivation-activation method is employed to simulate the excavation process and lining installation. The accuracy of finite element predictions is assessed through comparisons with available analytical solutions formulated in a simplified setting for the twin tunnels' configuration. A parametric study delves into the mutual interaction induced by tunnels proximity, emphasizing the crucial role of concrete lining stiffness in twin tunnels' deformation. Numerical simulations indicate a highly localized influence of a transverse gallery on twin tunnels deformation, extending up to four radii from each side of the gallery axis. Finally, the paper investigates the effects of twin tunnels proximity and those induced by an interconnecting gallery on the instantaneous and long-term convergence of tunnels, contrasting these outcomes with the convergence of a single tunnel.

1. Introduction

Many design methods often focus on single tunnels, but twin tunnels are a common occurrence. The interaction between tunnels can be significant, especially when the spacing between them is minimal. Additionally, many twin tunnels incorporate transverse galleries, introducing a localized effect on displacements and stresses. Also, the rheological behavior of the rock mass and lining plays a crucial role in how stress and displacements fields evolve over time. Some recent studies on deep twin tunnels can be found at [19, 6, 11, 7, 8, 12, 9, 10].

Chortis and Kavvadas [7] considered the calculation of the axial forces acting on the primary support in the intersection zone before, during, and after the construction of a perpendicular tunnel intersection. The results of the analysis indicated that the zone of influence extends approximately two diameters from the main tunnel to each side from the center of the intersection and that the interaction effects are practically eliminated when they exceed this delimited zone of influence.

In another study, Chortis and Kavvadas [8] carried out parametric 3D finite element analyses to verify the interaction between deep twin tunnel, with circular and non-circular cross-section, supported by a shotcrete lining, considering the rock mass with linear elastic behavior, perfectly plastic, with Mohr-Coulumb failure criteria, and the elastic linear lining. The study investigates the axial forces that develop in the primary lining of the twin tunnels as

*Corresponding author.

 motta.quevedo@ufrgs.br (Q.F.P. M.); ca-colombo@hotmail.com (C.C.A.M. M.); denise.bernaud@ufrgs.br (B. D.); samir.maghous@ufrgs.br (M. S.)

 <https://www.researchgate.net/profile/Felipe-Pinto-Da-Motta-Quevedo> (Q.F.P. M.);
<http://lattes.cnpq.br/4919388217690564> (C.C.A.M. M.); <http://lattes.cnpq.br/2809615143819128> (B. D.);
<https://www.researchgate.net/profile/Samir-Maghous> (M. S.)

ORCID(s): 0000-0003-4171-1696 (Q.F.P. M.); 0000-0001-6365-3269 (B. D.); 0000-0002-1123-3411 (M. S.)

a function of the main geometric and geomaterial parameters, but without considering the potential time-dependent deformations (creep effect) that occur in some types of rock masses.

Chen et al. [6], through analytical solutions in elasticity using complex variables, Fourier transformation, and the alternating Schwarz method, demonstrate that the mutual interaction between twin tunnels disappears if the spacing between the tunnels is greater than six times the tunnel radius. The lining effectively reduces the stress concentration, especially at high lateral stress coefficients.

Guo et al. [12] develop an elastic analytical solution for the stress field around twin circular tunnels with hydrostatic pressure using the complex variable and the superposition principle. They found that stress concentration in tunnel wall increased as the distance between the parallel tunnels and the pressure on the support decreased.

Ma et al. [13] proposed an analytical method, verified by a numerical solution using FLAC3D software for determining the plasticization zones around deep circular twin tunnels without linings, restricting themselves where there is no overlap between the two plastic zones. In this case, they adopted the perfectly plastic elastic constitutive model for the homogeneous and isotropic mass, with the Mohr-Coulomb criterion for the flow surface. They also carried out parametric studies to understand the influence of the distance between the twin tunnels, cohesion, the angle of internal friction, and the vertical and horizontal stresses acting on the shape and depth of the plastic zones. They recognizing the plastic zone around the tunnel provides a relevant theoretical basis for defining and designing the support. In addition, they mention that an excessive plastic zone significantly affects the stability and functionality of a tunnel. Therefore, the delimitation of the plastic zone around tunnels is of great importance for the development of projects.

Using parametric three-dimensional numerical analyses, Chortis and Kavvadas [9, 10] investigated the effect of building a transverse tunnel that intersected deep twin tunnels perpendicularly, focusing the study on the axial forces and the circumferential and longitudinal bending moments acting on the primary support of the intersection regions, respectively. According to the authors, the potential interaction between deep twin tunnels lined with shotcrete must be taken into account, especially when the distance between them is less than or equal to twice their diameter.

According to Fortsakis [11], in a realistic construction context, twin tunnels are excavated and supported with a delay, so that the second tunnel is usually built after the first one has advanced enough to maintain a longitudinal separation distance between the faces. The advance of the subsequent tunnel mobilizes the redistribution of stresses and deformations in the zone between the tunnels, resulting in additional loading of the preceding tunnel.

As for transverse tunnels, these are generally built far enough behind the advanced face of the main tunnel to ensure that their excavation has virtually no effect during the construction of the junction tunnel [7]. The interaction at the intersection, between the main tunnel and the transverse tunnel, significantly modifies the stress state of the primary support and that of the surrounding rock mass in these areas, compared to that of the singular tunnel, making three-dimensional finite element analyses essential for developing a realistic and safe design for tunnel junctions [19].

During the construction of the transverse tunnel, the surrounding rock mass is subjected to a redistribution of stresses, causing an additional load on the main tunnel, precisely in the intersection zone. If these additional loads exceed the load capacity of the primary support of the main tunnel, a potentially unstable region can develop, leading to failure, especially in adverse geotechnical conditions [7].

The long-term effect has been investigated for single tunnels, but little research has been done on twin tunnels, especially with a gallery. Therefore, in this work, the aim is to investigate the influence of the distance between the tunnels and the effect that the gallery has on the long-term convergence profile of deep-lined twin tunnels, considering various constitutive laws for the rock mass and the lining.

2. Fundamental assumptions

Despite the generality of the models, we employ some **delimitations** in this work:

- It is assumed only deep tunnels, neglecting surface influences such as deformations caused by surface loads and settlements arising from the excavation process;
- Although the inherent complexity of the rock mass's behavior, is influenced by spatially varying properties, this study opts for a simplified representation: a homogeneous and isotropic medium. While the rock mass may exhibit discontinuities, we simplify its overall behavior by treating it as a continuous medium. Consequently, the rock mass is considered single-phase and phenomenologically modeled using an elastoplastic-viscoplastic rheological law to capture instantaneous and long-term responses. This approach excludes considerations of other factors, such as temperature gradients, water flow, and pore mechanics;

- (c) Despite the complexity of the internal stress state of the rock mass, due, for example, to the discontinuities, anisotropy, and heterogeneity of the materials, equal vertical and horizontal stresses will be used, thus dealing with a geostatic-hydrostatic initial stress state.
- (d) It is common to design twin tunnels with a time lag between the excavation fronts. In this work, we will perform synchronous excavation, using symmetry conditions to minimize computer processing time.
- (e) In contrast to the variable conditions present in tunnel construction, where the excavation speed and lining installation fluctuate during the construction process, we adopt a constant speed for full, flat, and vertical excavation with homogeneous concrete lining with constant thickness. It's considered a constant humidity and temperature in the concrete lining.
- (f) We will not consider dynamic excitations (involving earthquakes and explosions, for example) and inertial terms (density and acceleration). In other words, the evolution of deformations occurs in a quasi-static manner. We also adopt the hypothesis of small perturbations.

3. Constitutive Model of the Rock Material

An elastoplastic-viscoplastic constitutive model was implemented in ANSYS using the UPF/USERMAT customization tool [1] to simulate rock mass. This model concerns the serial association of the plastic and viscoplastic constitutive models, i.e., the total strain $\dot{\epsilon} = \dot{\epsilon}^e + \dot{\epsilon}^p + \dot{\epsilon}^{vp}$, which leads to the following linear constitutive relationship:

$$\sigma = D : \dot{\epsilon}^e = D : (\dot{\epsilon} - \dot{\epsilon}^p - \dot{\epsilon}^{vp}), \quad (1)$$

where $\dot{\epsilon}^e$, $\dot{\epsilon}^p$ and $\dot{\epsilon}^{vp}$, represent the elastic, plastic and viscoplastic strain rate, respectively and D denote the fourth-order isotropic elastic linear constitutive tensor. The one-dimensional representation in Fig. 1 shows this association. In this

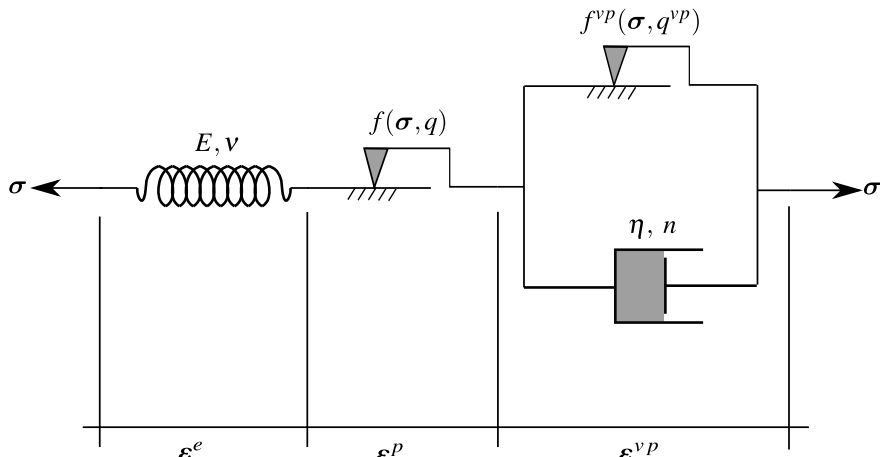


Figure 1: Rheological representation of the elastoplastic-viscoplastic model.

model is used a Drucker-Prager plastic flow surface given by

$$f(\sigma, q) = f(I_1, J_2, q) = \beta_1 I_1 + \beta_2 \sqrt{J_2} - q(\alpha), \quad (2)$$

which I_1 is the first invariant of the stress tensor, J_2 the second invariant of the deviator tensor and β_1 , β_2 and $q(\alpha)$ are strength parameters related to the friction angle ϕ and cohesion $c(\alpha)$, respectively. In the present model Drucker-Prager surface been inner of the Mohr-Coulomb surface [4], that is,

$$\beta_1 = \frac{(k-1)}{3}, \quad \beta_2 = \frac{(2k+1)}{\sqrt{3}}, \quad q(\alpha) = 2\sqrt{k} c(\alpha), \quad (3)$$

where $k = (1 + \sin \phi)/(1 - \sin \phi)$. The internal variable α is the equivalent plastic strain $\bar{\epsilon}^p$ used to simulate strain hardening/softening phenomena. However, for this study, we adopt perfect plasticity, meaning that c is a constant. For

the viscoplasticity surface f^{vp} the same surface is employed, but with ϕ^{vp} in β_1 and β_2 , and $q^{vp} = 2\sqrt{k^{vp}} - c^{vp}$ where $k^{vp} = (1 + \sin \phi^{vp})/(1 - \sin \phi^{vp})$ and c^{vp} is a constant, i.e., perfect viscoplasticity. The plastic flow rule is given by:

$$\dot{\epsilon}^p = \begin{cases} \lambda \frac{\partial g}{\partial \sigma} & \text{for } f > 0 \\ \mathbf{0}, & \text{for } f \leq 0 \end{cases}, \quad (4)$$

where λ is the plasticity multiplier and g is a potential function analogous to f to simulate the volume dilatation during the evolution of plastic deformations. However, for this analysis, was used associated plasticity, i.e., $g = f$. The plastic multiplier is obtained through the consistency condition $\dot{f} = 0$. Numerical details of this implementation can be found in [18]. For viscoplastic flow rule we have,

$$\dot{\epsilon}^{vp} = \lambda^{vp} \frac{\partial f^{vp}}{\partial \sigma} \quad (5)$$

In contrast to the plastic multiplier, the viscoplastic multiplier λ^{vp} is independent of a consistency condition. As a result, its expression is explicit. For this study, we utilize the Perzyna model as follows:

$$\lambda^{vp} = \frac{\Phi(\sigma, q^{vp})}{\eta} \quad \text{and} \quad \Phi = \left\langle \frac{f^{vp}(\sigma, q^{vp})}{f_0} \right\rangle^n, \quad (6)$$

where Φ is the overstress function, η is the dynamic viscosity constant, n is the dimensionless parameter that gives the form of the power law, f_0 a parameter conveniently adopted and $\langle \cdot \rangle$ is the McCauley function which is 0 when $\cdot < 0$, i.e. viscoplastic flow will only occur when the overstress function is positive.

In this coupled model, when $\phi = \phi^{vp}$, cohesion entirely controls the evolution of local mechanical fields. Specifically, when $c \rightarrow \infty$ and $c^{vp} \rightarrow \infty$, the system achieves a purely elastic solution. The solution becomes purely elastoviscoplastic with $c \rightarrow \infty$, while a pure elastoplastic solution emerges with $c^{vp} \rightarrow \infty$. In this study's coupled analysis, we have adopted $c^{vp} < c$, allowing the viscoplastic domain to occur without plasticity. However, in the presence of plasticity, viscous effects become inevitable. Fig. 2 illustrates these domains in principal stress space.

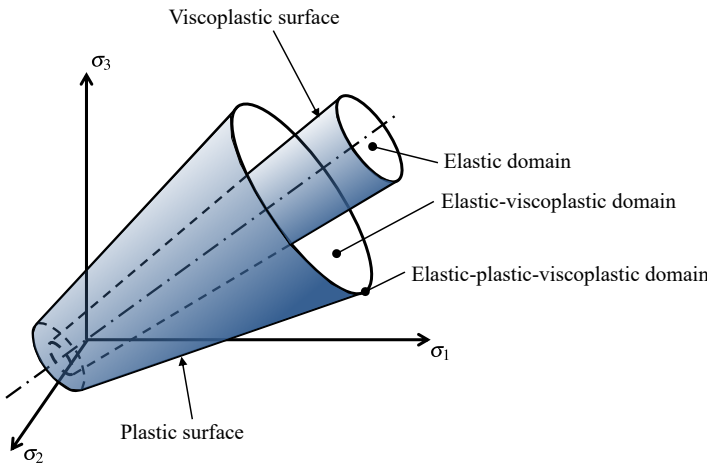


Figure 2: Elastoplastic-viscoplastic domains.

Details of this model, including validations and its application in single tunnel, are in [18]. See [16] for the algorithm details implemented in FORTRAN within the USERMAT subroutine.

4. Constitutive Model of the Lining

We implemented a viscoelastic model in ANSYS using the UPF/USERMAT customization feature [1]. The model simulates concrete creep through a Generalized Kelvin chain, based on Bažant and Prasannan's Solidification Theory

[2; 3], with parameter adjustments performed using the CEB-FIP MC90 formulation. The CEB-FIP MC90 formulation also [5] determines the shrinkage component.

In this model, the constitutive relationship between stress and strain is

$$\boldsymbol{\sigma} = \mathbf{D} : \dot{\boldsymbol{\epsilon}}^e = \mathbf{D} : \dot{\boldsymbol{\epsilon}} - \mathbf{D} : \dot{\boldsymbol{\epsilon}}^{sh} - \mathbf{D}^* : \dot{\boldsymbol{\epsilon}}^{cr} \quad (7)$$

where $\dot{\boldsymbol{\epsilon}}^{sh}$ and $\dot{\boldsymbol{\epsilon}}^{cr}$ are the shrinkage and creep strain rate, respectively, while \mathbf{D} and \mathbf{D}^* denote the fourth-order isotropic elastic linear constitutive tensor and modified constitutive tensor that incorporates the aging of the concrete, respectively. Due to the time integration scheme for the Newton-Raphson algorithm, the Eq. (7) is given by:

$$\boldsymbol{\sigma}_{n+1} = \boldsymbol{\sigma}_n + \mathbf{D} : \Delta\boldsymbol{\epsilon} - \mathbf{D} : \Delta\boldsymbol{\epsilon}^{sh} - \mathbf{D}^* : \Delta\boldsymbol{\epsilon}^{cr} \quad (8)$$

in which the increment of shrinkage strain is:

$$\Delta\boldsymbol{\epsilon}^{sh} = \Delta\boldsymbol{\epsilon}_{sh}(t_s)\mathbf{1} \quad (9)$$

where t_s represents the concrete curing time, and $\Delta\boldsymbol{\epsilon}_{sh}$ is the variation of magnitude of the concrete deformation by shrinkage, determined using the expressions of CEB-FIP MC90 [5]. To calculate the increment of creep strain, denoted as $\Delta\boldsymbol{\epsilon}^{cr}$, we use the incremental algorithm developed by Bažant and Prasannan [2; 3], with an adjustment to incorporate CEB-FIP MC90 formulation. This adaptation is possible comparing the creep functions $J(t, t_0)$ of both references. This gives to the following equivalence:

$$E_0 = E_c(t_0), \gamma_c(t - t_0) = \beta_c(t - t_0), \frac{1}{v(t)} = \frac{\phi_0}{E_{ci}} \text{ and } \frac{1}{\eta(t)} = 0 \quad (10)$$

in which, according to Bažant and Prasannan [2; 3], E_0 is the modulus of elasticity of the concrete aggregates and microscopic particles of the cement paste, $\gamma_c(t - t_0)$ is the microviscoelastic deformation of the volume fraction of solidified concrete $v(t)$, $\eta(t)$ is the apparent macroscopic viscosity and, according to CEB-FIP MC90 [5], $E_c(t_0)$ is the tangent elastic modulus of the concrete at the instant of loading application t_0 , $\beta_c(t - t_0)$ is a coefficient that depends on the loading age $t - t_0$, ϕ_0 is a coefficient that depends on the age of the concrete at the instant of loading application and E_{ci} the tangent elasticity modulus of the concrete at the age of 28 day.

Details of this model, including validations and its application in single tunnel, are in [17]. See [15] for the algorithm details implemented in FORTRAN within the USERMAT subroutine.

5. Spatial and time discretization of the domain

The problem domain Ω consists of a twin deep tunnel with a cross gallery, as shown in Fig. 3.

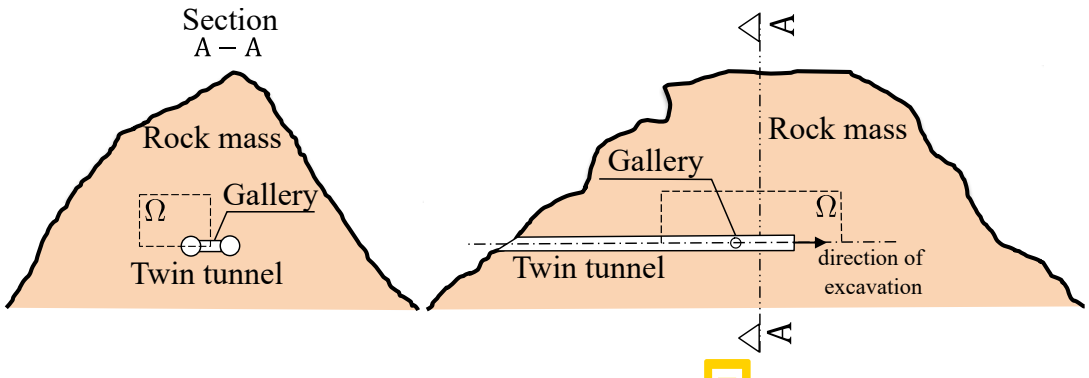


Figure 3: Problem domain

The spatial discretization of the domain Ω corresponds to a mesh with trilinear hexahedral elements (SOLID 185, 8 nodes), except in the gallery region, which uses higher-order tetrahedral elements (SOLID186, 10 nodes). Fig. 4 shows the mesh, geometric parameters, and boundary conditions for the domain problem. We considered front, side, and

bottom symmetry to reduce computational cost. In this discretization, d_1 is the distance between longitudinal tunnel axes, R_i radius of the longitudinal tunnel, L_2 total excavated length, d_3 domain height, L_1 length of the unexcavated region, L_3 transversal length of the domain, L_p step length of the excavation process, d_2 position of the gallery along the longitudinal tunnel. In conjunction with boundary pressure p , we apply the initial stress condition $\sigma_0 = -p\mathbf{1}$ at all integration points to simulate the initial state of an undisturbed rock mass. We divided the mesh into two regions:

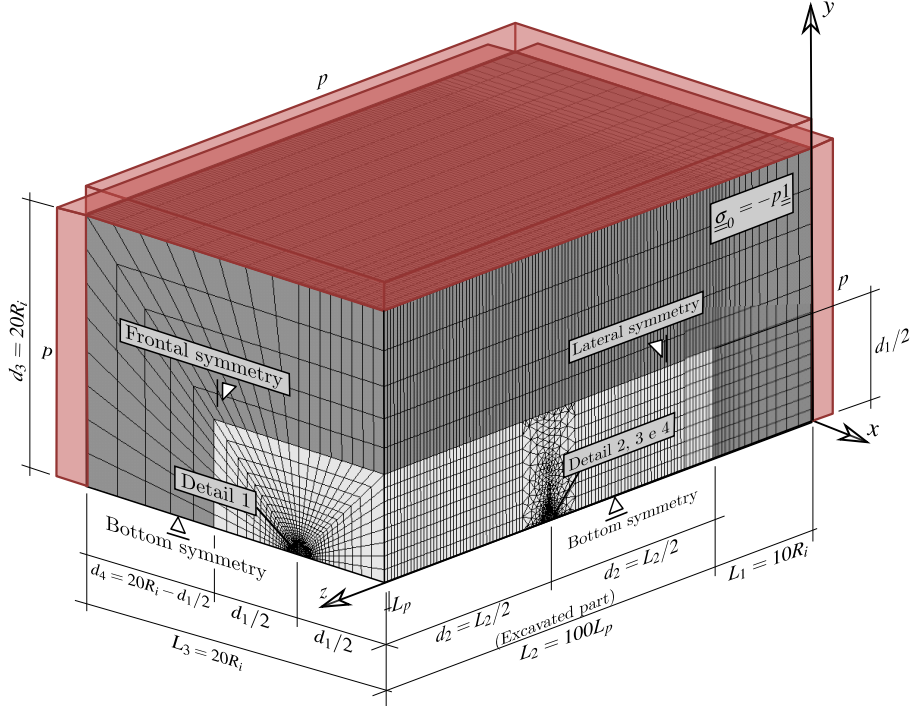


Figure 4: Mesh, dimensions and boundary conditions of the 3D twin tunnel domain

one near the tunnel (light gray), which we refined more, and a region farther away (dark gray), which we increased the aspect ratio to minimize the number of elements in that region. Due to the low deformation gradient away from the tunnel wall, elements in this area can be considerably larger than in other regions. Fig. 5 presents the mesh at the cross-section of the longitudinal tunnel, with e representing the thickness of the lining

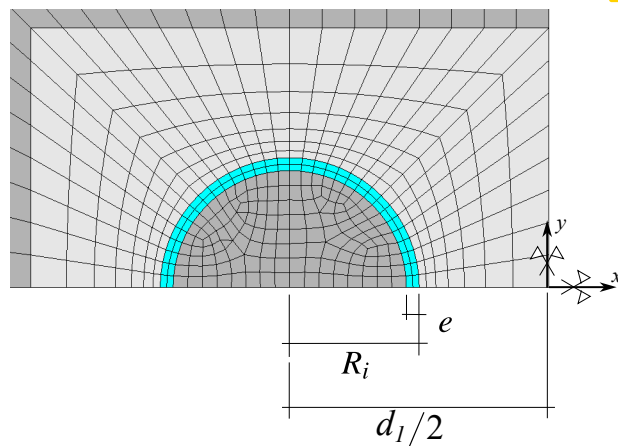


Figure 5: Detail 1 - Mesh in longitudinal tunnel cross-section with spacing $d_1 = 4R_i$



One of the aspects investigated in this work is the influence of the spacing d_1 between longitudinal tunnels of the twin tunnel. Fig. 6 and Fig. 7 illustrate the spatial discretization in the gallery region and its connection with the longitudinal tunnel considering spacings $d_1 = 16R_i$, $8R_i$ and $4R_i$, respectively. We adopt the radius of the gallery as $2/3R_i$, and its lining has the same thickness as the longitudinal tunnel. The dimensions d_5 and d_1 define the size of the transition region comprising tetrahedral elements between the gallery and the rest of the domain. Fig. 8 shows half of this transition region inside the rock mass.

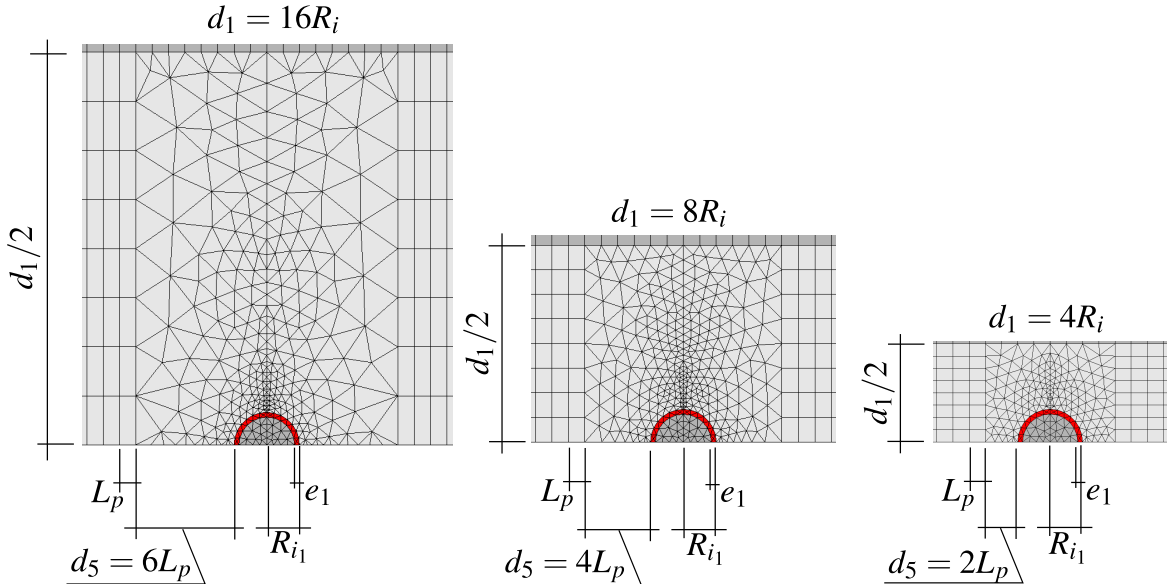


Figure 6: Detail 2 - Side view of the mesh in gallery region with $d_1 = 16R_i$, $d_1 = 8R_i$ and $d_1 = 4R_i$

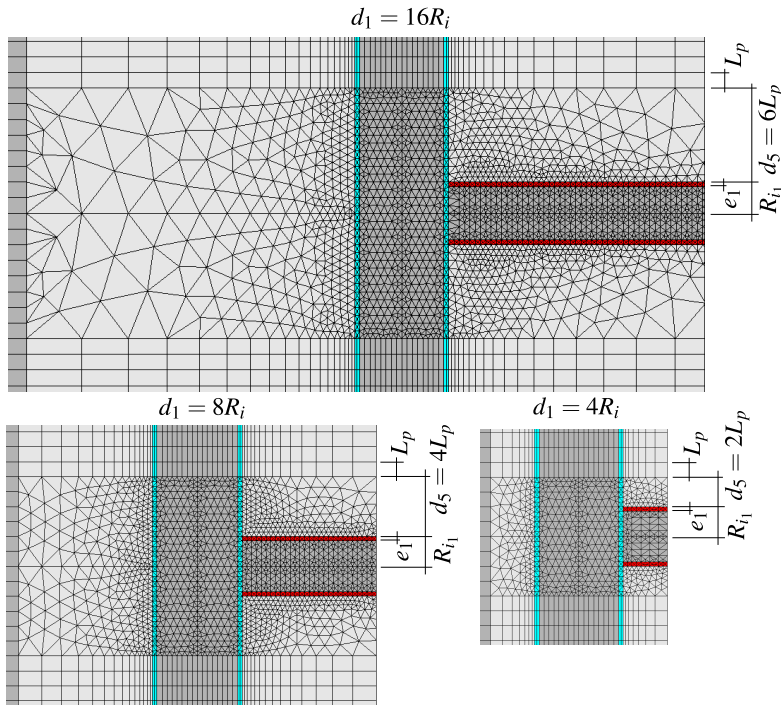


Figure 7: Detail 3 - Bottom view of the mesh in gallery region with $d_1 = 16R_i$, $d_1 = 8R_i$ and $d_1 = 4R_i$

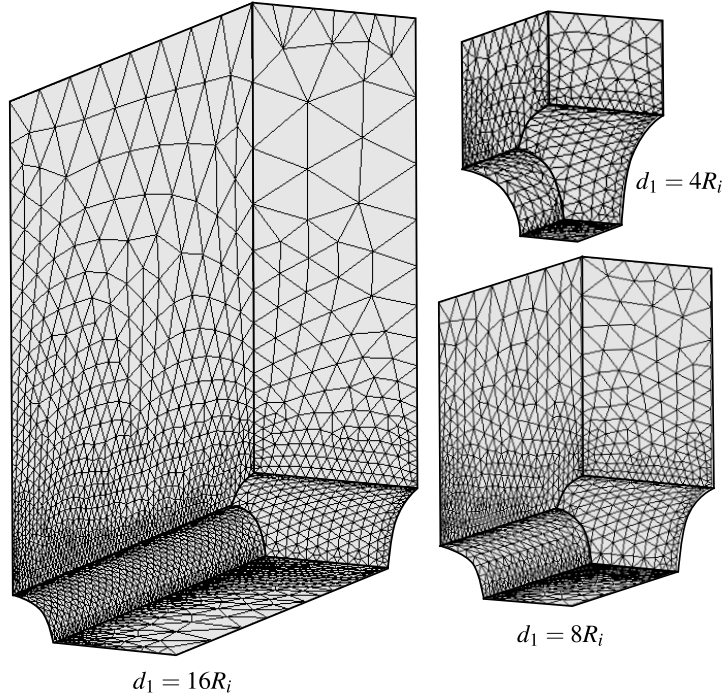


Figure 8: Detail 4 - Isometric view of the portion of the mesh in gallery transition region $d_1 = 16R_i$, $d_1 = 8R_i$ and $d_1 = 4R_i$

Fig. 9 shows the mesh of the lining at the junction of the gallery and the longitudinal tunnel for $d_1 = 4R_i$, $8R_i$, and $16R_i$. One noteworthy characteristic of this mesh is that it confines the tetrahedral elements within the contour of every excavation step.

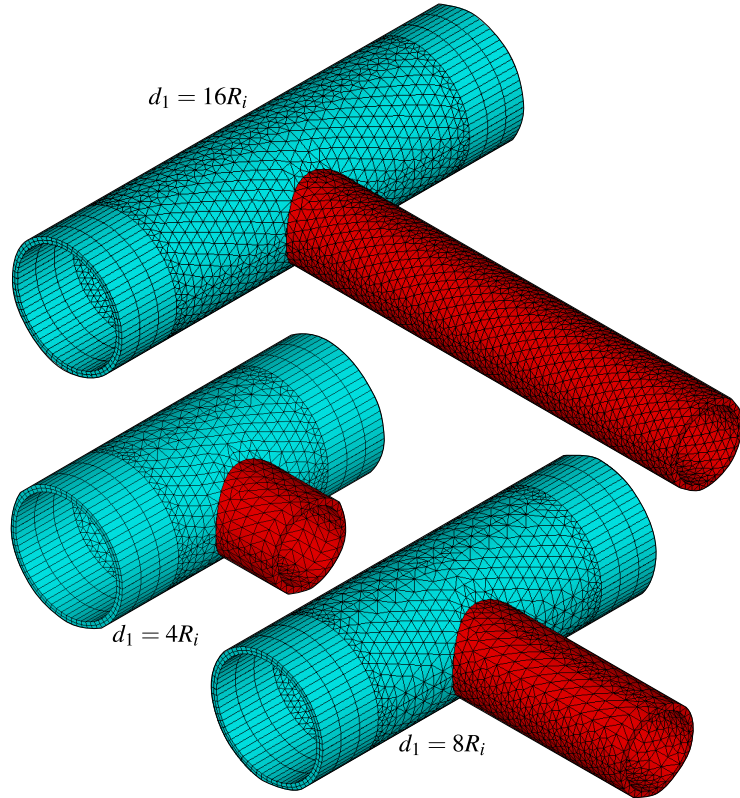


Figure 9: Isometric view of the lining at the intersection for $d_1 = 16R_i$, $d_1 = 8R_i$ and $d_1 = 4R_i$ - expansion of symmetry in the xz plane

The construction process is simulated through the deactivating and activating method, i.e., in each step of excavation, reducing the stiffness of the excavated element (multiply by 1E-8) and active the lining elements at a distance d_0 from the excavation face (unlined length). With each excavation step, we execute the solution, and time advances based on the expression $t_p = L_p/V_p$, where L_p represents the length of the excavation step, and V_p is the speed of the excavation face. Fig. 10 illustrates a schematic of the excavation process where n_p is the number of excavation steps. In this Figure, n_{pig} represents the number of steps excavated in the longitudinal tunnel that starts gallery excavation. Once reaching this step, we pause the excavation of the longitudinal tunnel, and the gallery excavation begins. In the gallery, L_{p1} is the step length of the gallery excavation, V_{p1} is the speed of the gallery excavation, and d_{01} is the unlined length of the gallery. After completing the gallery excavation, the longitudinal tunnel excavation resumes. These parameters related to the geometry domain, excavation and installation of the lining are shown in Table 1.

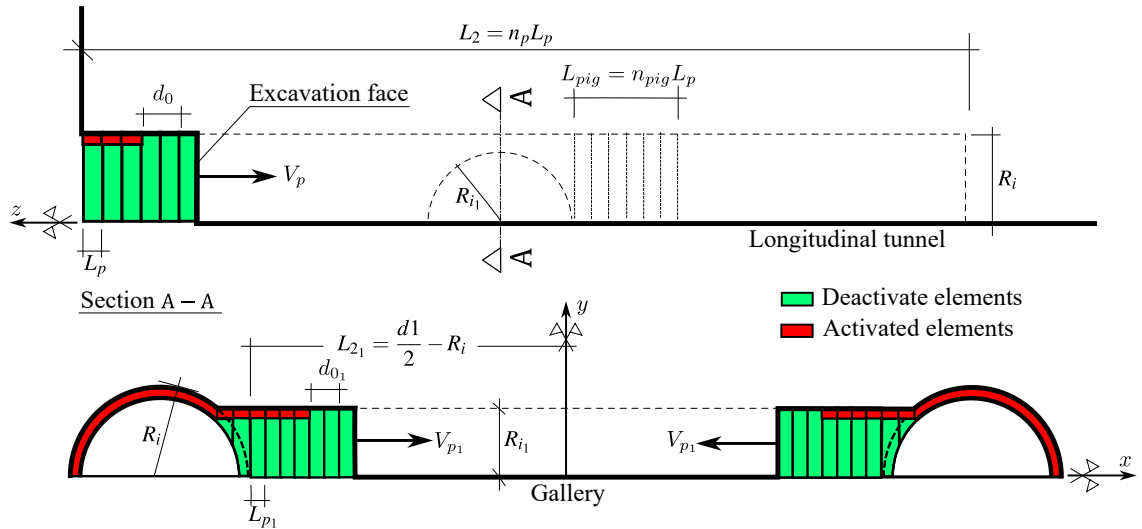


Figure 10: Schematic of the excavation process

Table 1

Parameters related to the geometry of the domain, excavation and installation of the lining

PARAMETERS	SYMBOL	UNIT	VALUES
Longitudinal tunnels			
Radius of the longitudinal tunnel	R_i	m	1
Thickness of the lining	e	m	0.1 R_i
Step length of the excavation process	L_p	m	$1/3 R_i$
Unlined length	d_0	m	$2L_p$
Speed of the excavation face	V_p	m/day	12.5
Excavation step time	t_p	day	L_p/V_p
Gallery			
Radius of the gallery	R_{i1}	m	$2L_p$
Thickness of the lining	e_1	m	$0.1R_i$
Step length of the excavation process ¹	L_{p1}	m	$0.3R_{i1}$ $0.3214R_{i1}$ $0.3387R_{i1}$
Unlined length	d_{01}	m	$2L_{p1}$
Speed of the excavation face	V_{p1}	m/day	12.5
Number of steps that starts gallery excavation	n_{pig}	un	15
Rest of domain			
Distance between longitudinal tunnel axes	d_1	m	$4R_i$ $8R_i$ $16R_i$
Length of the unexcavated region	L_1	m	$10R_i$
Total excavated length	L_2	m	$100L_p$
Domain height	L_3	m	$20R_i$

¹ $L_{p1} \approx 1/3R_{i1}$ in such a way that there are n integer excavation steps in $d_1 - 2R_i$

During tunnel construction, we determine the initial time increment for solution steps as $0.5t_p$ (for the longitudinal tunnel) and $0.5t_{p_1}$ (for the transverse gallery). ANSYS manages the time increment using the bisection method, halving the time step if there is no equilibrium convergence.

After tunnel excavation, in time-dependent constitutive models, time continues to progress to capture long-term viscous effects. In this stage, each time step lasts 100 days, with an initial increment of 50 days. This increase, compared to the excavation time increments, is facilitated by the semi-implicit scheme in the viscoplasticity solution. The explicit scheme, as indicated in [20], requires a smaller time increment to the precision of the solution.

6. Comparision with analytical solutions

To examine mesh convergence and validate the numerical model, we compared the numerical solution with the elastic and elastoplastic analytical solution in the plane state of deformations for twin tunnels. Guo et al. [12] develop an elastic analytical solution for the stress field around twin circular tunnels with hydrostatic pressure using the complex variable and the superposition principle. The Fig. 11 shows the tangential stress distribution around the tunnel's boundary in this analytical solution with the numerical solution considering $R_i = 4$ m, $E = 500$ MPa, $\nu = 0.23$, $d_1 = 2R_i$, $p = 2.2$ MPa.

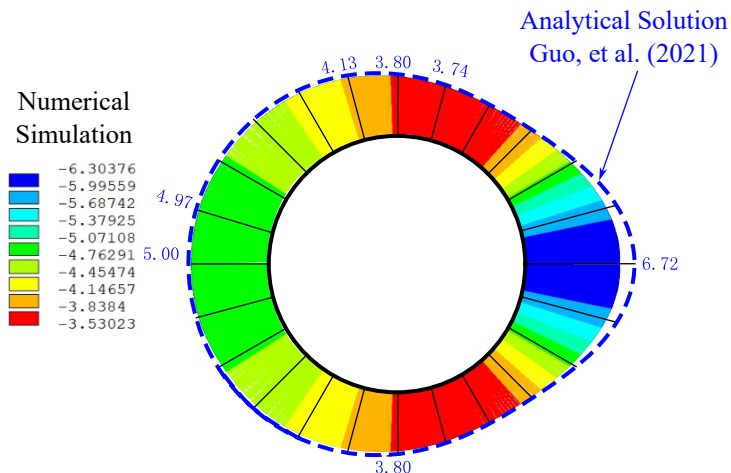


Figure 11: Verification of numerical results of orthoradial stresses with the analytical solution

Ma et. al. [13] developed an analytical solution for a perfectly plastic constitutive model with a Mohr-Coulomb surface. One of the results was the contour of the plastic zone for several conditions. Fig. 12 shows the comparison between the numerical model solution (taken from a section away from the excavation face) and the analytical solution. For these analysis, $R_i = 1$ m, Young's modulus $E = 20$ GPa and Poisson's ratio $\nu = 0.3$.

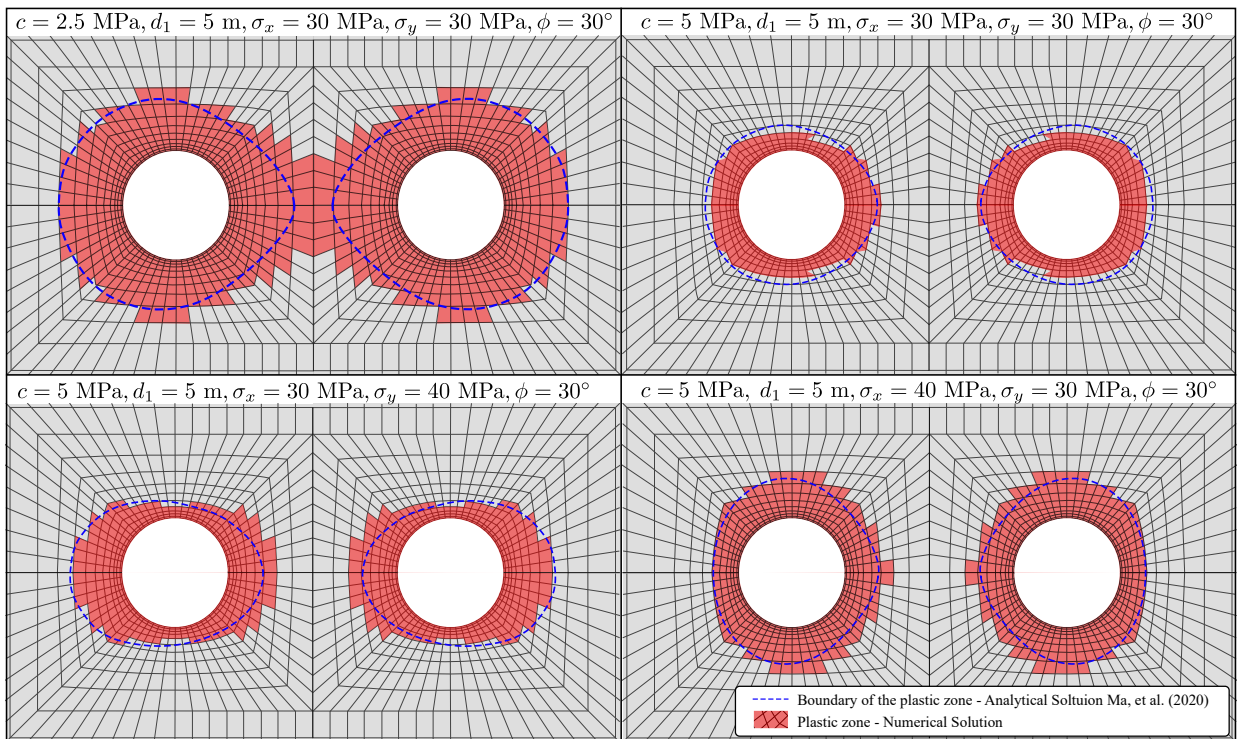
**Figure 12:** Numerical and analytical comparison of plastic zones

Fig. 13 displays the magnitude of displacements, radial, σ_r , σ_θ , σ_z , and z-direction stresses at the element level for the case with $c = 5 \text{ MPa}$, $d_1 = 5 \text{ m}$, $\sigma_x = \sigma_y = 30 \text{ MPa}$. We adopted a case without excavating the gallery to assess the quality of the mesh. The smoothness observed in the solution between the elements indicates satisfactory discretization.

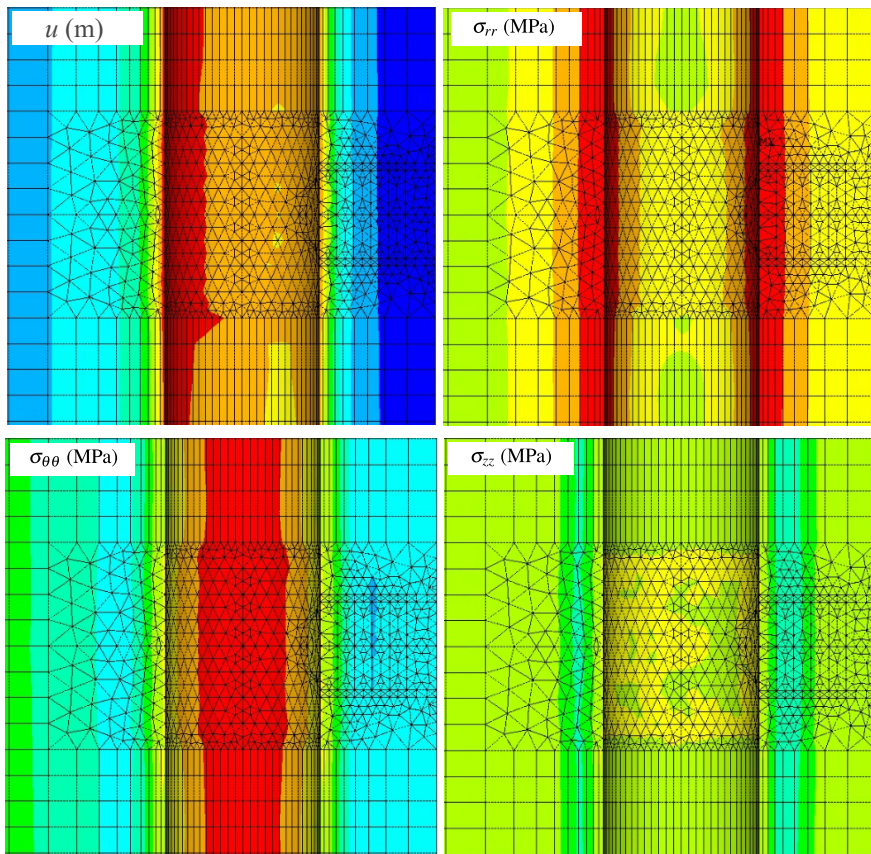


Figure 13: Element solution with $c = 5$ MPa, $d_1 = 5$ m, $\sigma_x = \sigma_y = 30$ MPa

7. Numerical Results and Discussion

To develop the parametric analyses, we utilized the constitutive parameters of the rock mass as outlined in Piepi [14], and for the lining, we employed typical values for ordinary reinforced concrete. These parameters are shown in Table 2. In these analyses, an isotropic initial stress state of 9 MPa is considered, and the excavation speed is 12.5 m/day [14].



Table 2

Constitutive parameters used in the parametric analysis

PARAMETERS	SYMBOL	UNIT	VALUES
Constitutive model of rock mass			
Young's modulus	E	MPa	1500
Poisson's ratio	ν	adm	0.498
Plastic cohesion	c	MPa	$4\sqrt{3}/2$
Plastic friction angle	ϕ	°	0
Viscoplastic Cohesion	c_{vp}	MPa	$2\sqrt{3}/2$
Viscoplastic friction angle	ϕ_{vp}	°	ϕ
Power law parameter	n	adm	1
Reference parameter	f_0	MPa	1
Viscosity coefficient	η	day	40000
Constitutive model of lining			
Compressive strength	f_{ck}	MPa	20
Young's modulus at 28 days	$E_{c_{28}}$	MPa	30303
Poisson's ratio	ν	adm	0.3
Coefficient which depends on the type of cement	s	adm	0.2
Relative humidity of ambient environment	RH	%	70
Fictitious thickness (longitudinal tunnel)	h_f	cm	0.2111
Fictitious thickness (transverse gallery)	h_f	cm	0.2176
Drying time of the concrete	t_s	days	7
Coefficient in shrinkage which depends on the type of cement	β_{sc}	adm	8
Temperature	T	°C	20°
Age of concrete at loading	t_0	days	1

In presenting the results, U_{eq} denotes the equilibrium convergence value at the convergence profile outside the region of influence of the excavation face and the gallery. When the gallery is present, the highest convergence value, U_{peak} is highlighted at the gallery position. In addition, it is necessary to highlight some important points:

- **Observation 1:** All the results presented in the following analyses pertain to the point located at the top of the tunnel section (crown), and we will monitor its convergence throughout the excavation process. Fig. 14 presents this point. Likewise, we will only analyze the convergence of the point located at the crown of the gallery.
- **Observation 2:** Under material isotropy and initial stress state, the symmetry of the tunnel wall is preserved throughout the excavation process. Thus, the deformed tunnel wall remains circular. On the other hand, one of the effects of the mutual interaction induced by the proximity of the tunnels is the loss of symmetry of the deformed tunnel wall, as illustrated in Fig. 14. In this context, the point chosen to follow the convergences (on the crown) is not representative of the entire deformation of the tunnel wall.
- **Observation 3:** Referring to the material properties shown in Table 2, the value adopted for plastic cohesion (c) is higher than the value for viscoplastic cohesion (c_{vp}): $c > c_{vp}$. This implies that in the regime of irreversible deformations, the viscoplasticity of the material will be activated first. Throughout the excavation process, viscoplastic deformations will appear without plasticization of the massif. The generic configurations of the deformation zones of the massif throughout the excavation process are illustrated in Fig. 15.

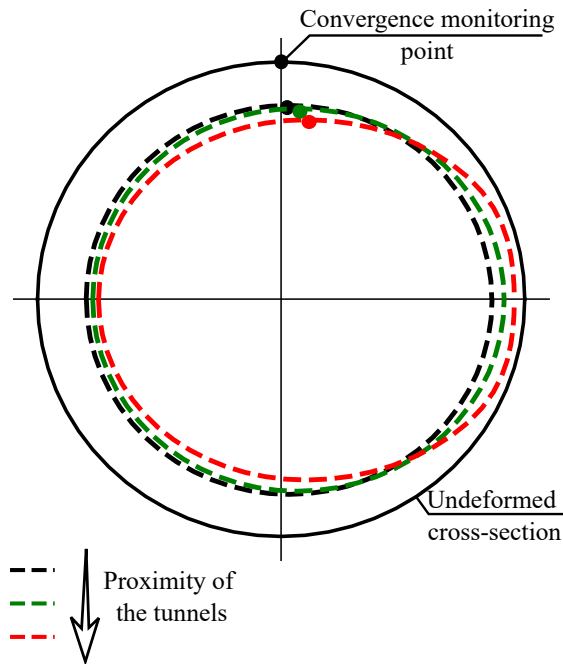


Figure 14: Monitoring point and ovalization effect

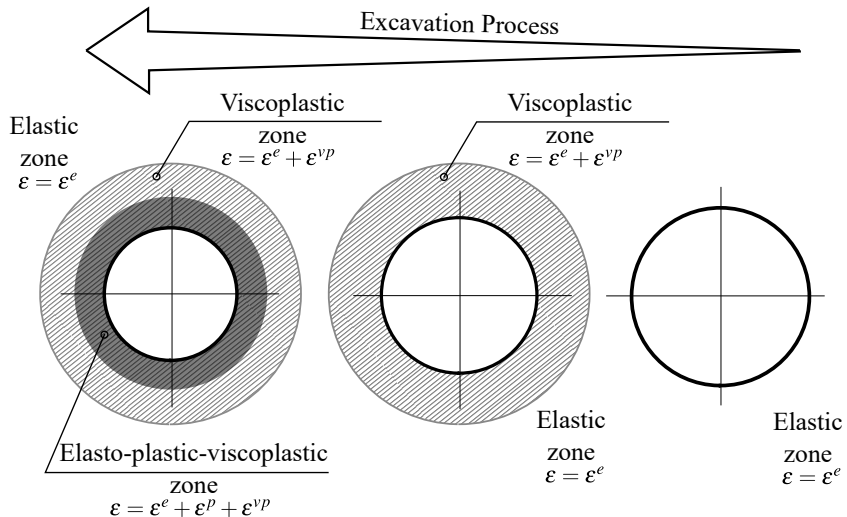


Figure 15: Configurations for the zones with irreversible deformations in the rock mass

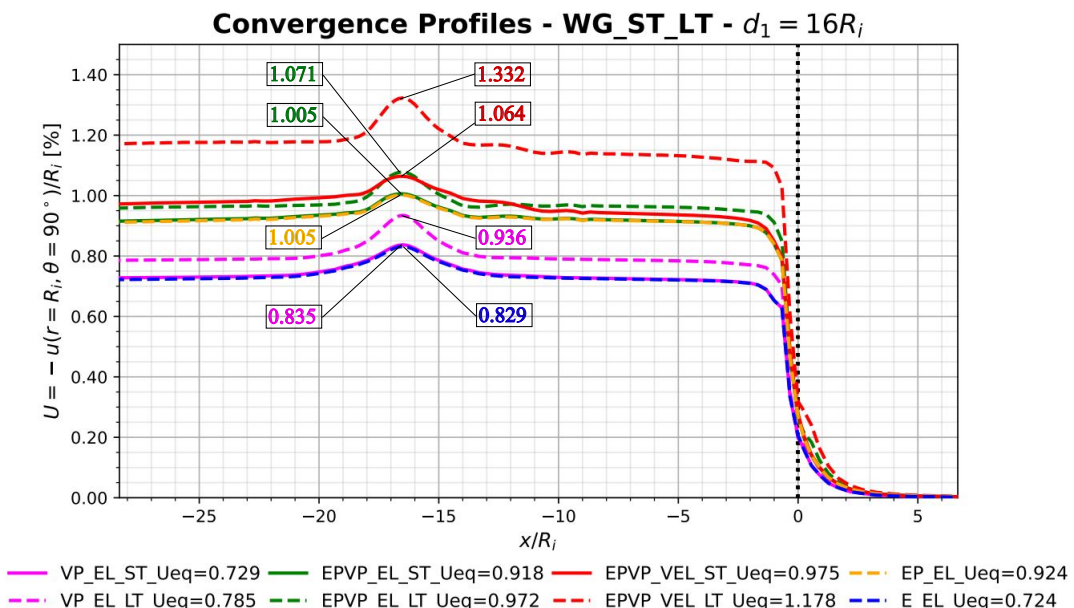
Table 3 presents the abbreviation to read the title and legend of the results.

Table 3

Abbreviation to the title and legend of the results

DESCRIPTION	ABBREVIATION
Elastic rock mass	E
Elastoplastic rock mass	EP
Elastoviscoplastic rock mass	VP
Elasto-Plastic-Viscoplastic rock mass	EPVP
Not lining	NL
Elastic lining	EL
Viscoelastic lining	VEL
Long-term	LT
Final excavation (Short-term)	ST
With Gallery	WG
Not Gallery	NG

Figs. 16, 17, and 18 show the convergence profiles of the twin tunnels with gallery (WG) for all the constitutive models of the rock mass (E - blue, EP - yellow, VP - magenta, EPVP - red) and the lining (EL and VEL) in the short-term (solid lines) and the long-term (dashed lines), for $d_1 = 16R_i$, $8R_i$ and $4R_i$ respectively.

**Figure 16:** Convergence Profiles - with gallery (WG), short-term (ST) and long-term (LT) for $d_1 = 16R_i$

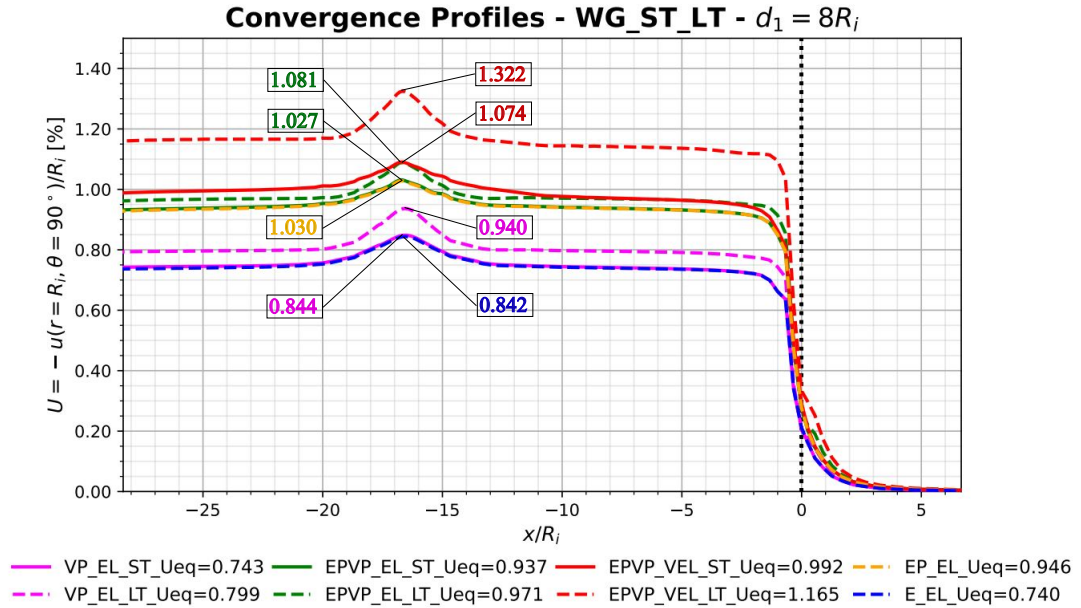


Figure 17: Convergence Profiles - with gallery (WG), short-term (ST) and long-term (LT) for $d_1 = 8R_i$

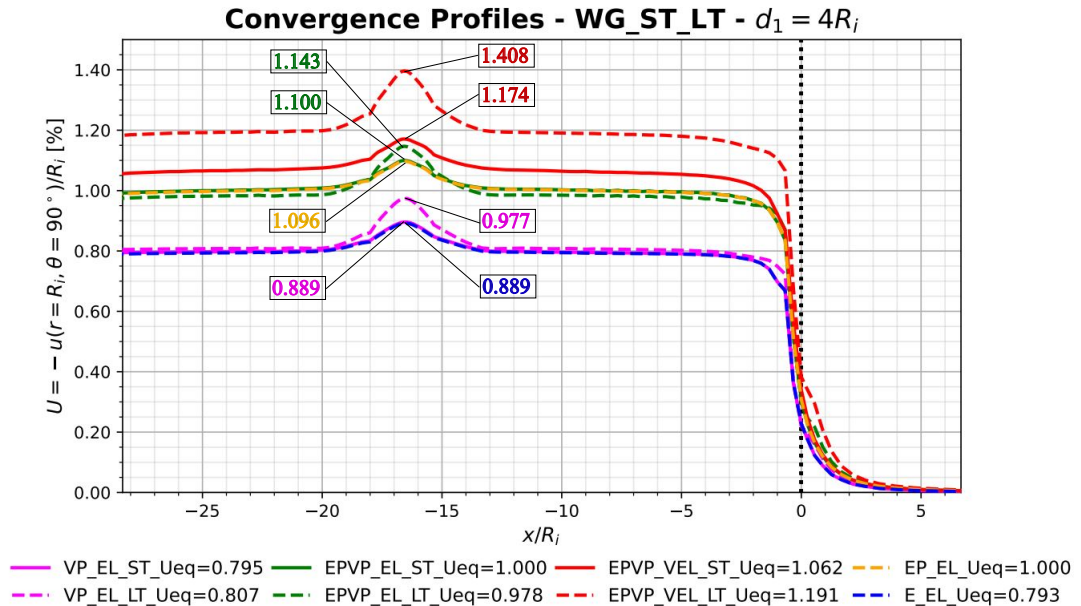


Figure 18: Convergence Profiles - with gallery (WG), short-term (ST) and long-term (LT) for $d_1 = 4R_i$

In all d_1 distances, the convergence profiles of the E-EL model (blue dashed line) and the VP-EL (magenta solid line) in the short-term (ST) are equivalent, probably due to the high excavation speed. The high speed of the excavation and installation of the lining limits the time for the viscous effects to manifest themselves also taking into account the restriction imposed by the stiffness of the lining.

In the short-term (ST), the EPVP-EL model (green solid line) is equivalent to the EP-EL (yellow dashed line) because, although plasticization around the section has already occurred due to excavation, the viscous effects have not yet evolved considerably due to the short time variation between the start of excavation and the end of the excavation process. After the long-term convergence occurs (green dashed line) are a difference. However, when the rheological effect of the lining is present, the profile continues to evolve considerably over the long-term, for example, EPVP-VEL (red solid and dashed line).

It's worth noting that the stiffness of the elastic lining significantly impedes the evolution of convergence due to viscous effects, particularly evident in the VP-EL model with $d_1 = 4R_i$ (magenta solid and dashed line). In this scenario, the interaction between nearby twin tunnels causes a substantial rise in the value of U_{eq} in the short-term (ST). However, the profile in the long-term (LT) practically remains unchanged, staying close to the short-term due to the limitation imposed by the stiffness of the lining.

Another noteworthy aspect is that the EPVP-VEL model with $d_1 = 16R_i$ (red dashed line) experiences a reduction in U_{eq} convergence after 15 excavation steps (n_{pig}) following the gallery. This phenomenon is due to the evolving viscous effects of the already-excavated longitudinal tunnel during the gallery excavation. This effect becomes more pronounced with $d_1 = 16R_i$. When the gallery is smaller ($d_1 = 8R_i$ and $4R_i$), the time elapsed is shorter, and this effect is less pronounced.

Note another aspect: the EPVP-EL-LT (green solid line) model converges slightly lower than the EVP-EL-ST (green dashed line) model with $d_1 = 4R_i$. The ovalization effect is responsible for the crown's convergence decreasing over time. However, another point in the section experiences an increase in convergence. Fig. 19 illustrates this effect away from the gallery region with a single tunnel reference.

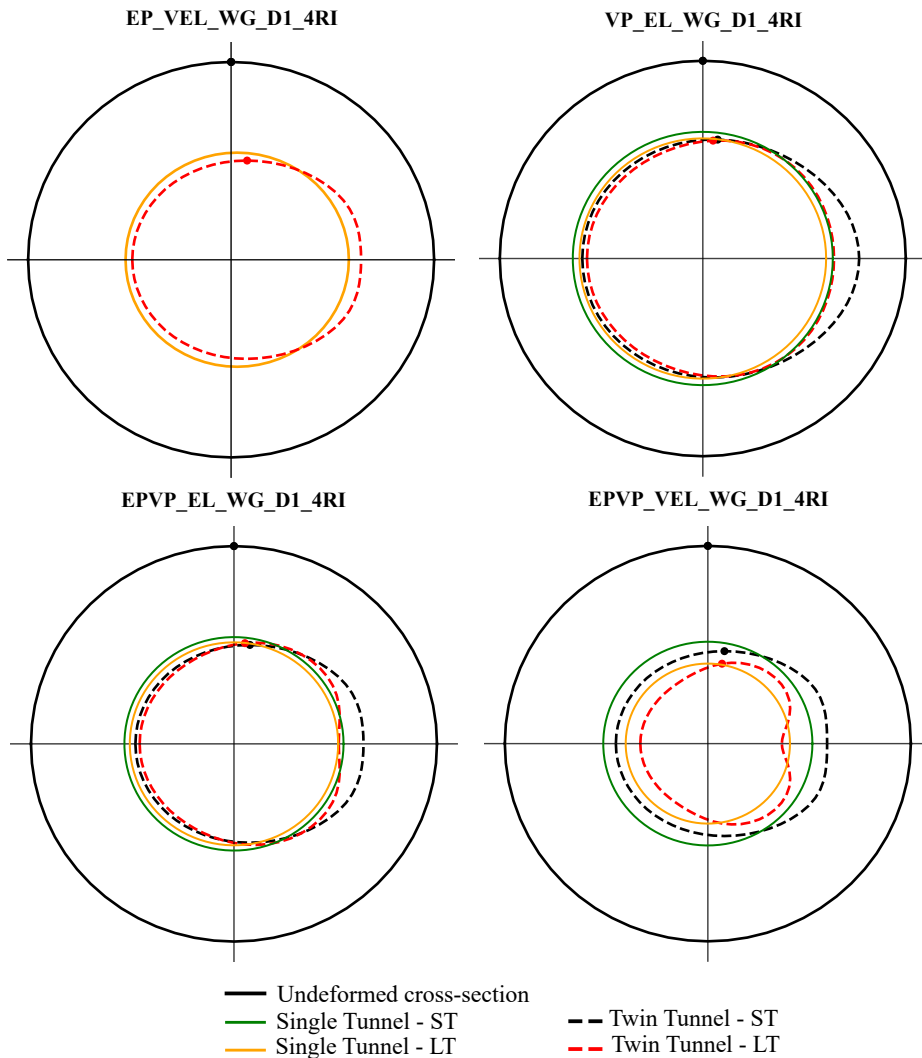


Figure 19: Ovalization effect for $d_1 = 4R_i$ scaled 50x

Fig. 20 compares the convergence profiles of the viscoplastic rock mass (VP) with elastic lining (EL) models (solid lines) with the elasto-plastic-viscoplastic rock mass (EPVP) with elastic (EL) and viscoelastic lining (VEL) models in the long-term (LT) (dashed lines and dot lines, respectively). As a reference, it also shows the results for a single tunnel (black lines).

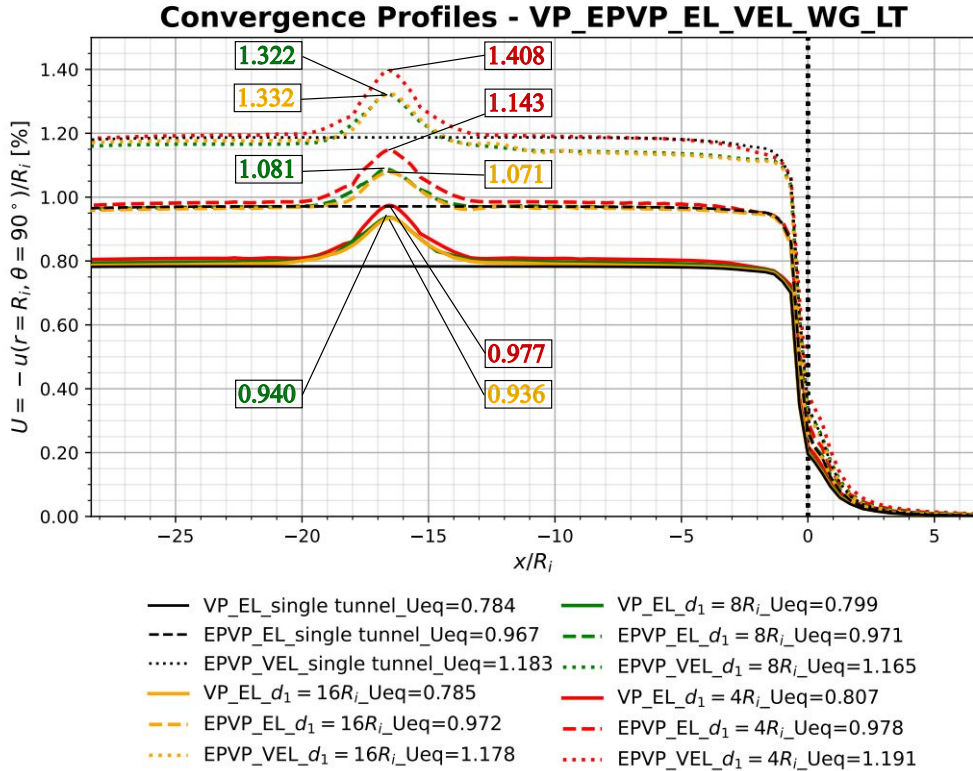


Figure 20: Convergence Profiles - viscoplastic rock mass (VP) with elastic lining (EL) versus elasto-plastic-viscoplastic rock mass (EPVP) with elastic (EL) and viscoelastic lining (VEL) in long-term (LT)

Figure 20 shows a slight increase in the peak value of convergence U_{peak} for the EPVP-VEL model when comparing $d_1 = 16R_i$ (dotted yellow line) and $d_1 = 8R_i$ (dotted green line). In the case of $d_1 = 8R_i$, the proximity of the tunnel compensates the convergence difference due the gallery excavation elapsed time between $d_1 = 8R_i$ and $16R_i$. However, when $d_1 = 4R_i$ (dotted red line) the effect of the gallery is more pronounced due to the interaction between the proximity of the twin tunnels and the viscous effect.

Moreover, one can observe a more pronounced effect in the section before the gallery, specifically at the plateau of the convergence profile, in the EPVP-VEL model for $d_1 = 8R_i$ and $d_1 = 16R_i$ (green and yellow dotted lines). This effect is due to the viscoelastic behavior of the lining and elapsed time to excavate the gallery. Unlike the highly rigid elastic lining, the viscoelastic lining allows the convergence to evolve during the excavation of the gallery. Consequently, the values of convergences before the gallery tend to be higher than after the gallery.

Fig. 21 compares the convergence profiles of the elastoplastic rock mass (EP) and elastic lining (EL) models (solid lines) with the elasto-plastic-viscoplastic rock mass (EPVP) and viscoelastic lining (VEL) models in the short-term (ST) (dot lines) and long-term (LT) (dashed lines). As a reference, it also shows the results for a single tunnel (black lines).

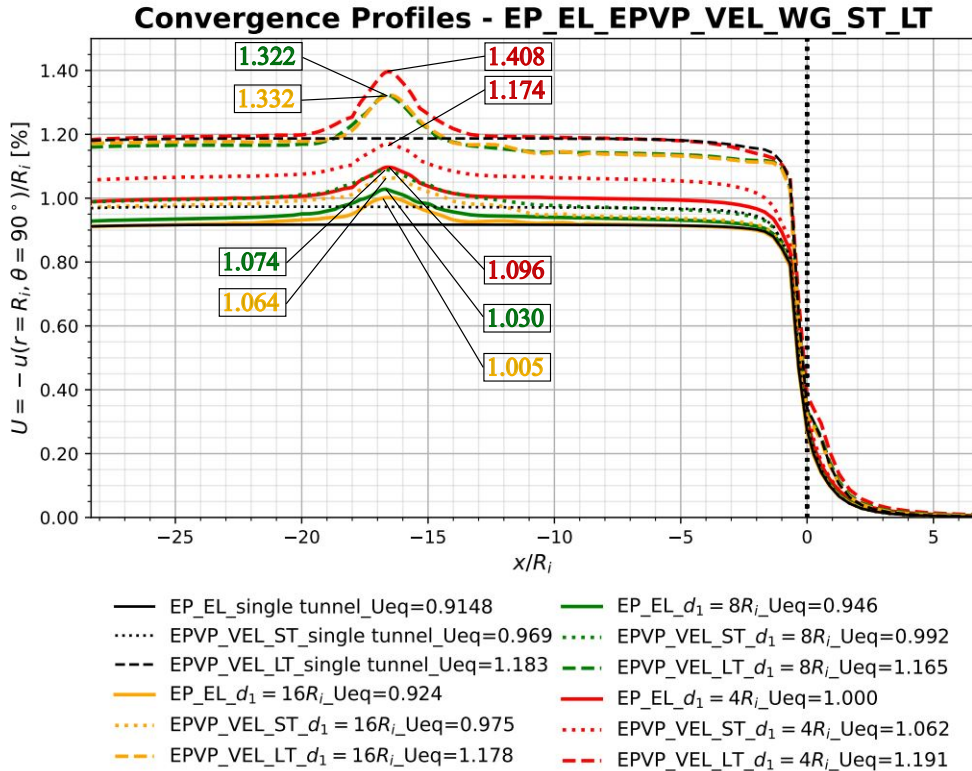


Figure 21: Convergence Profiles - elastoplastic rock mass (EP) with elastic lining (EL) versus elasto-plastic-viscoplastic rock mass (EPVP) with viscoelastic lining (VEL) in short-term (ST) and long-term (LT)

This Figure shows the crucial effect of the viscoelastic lining to the convergence profile of the tunnels. In the short term (ST), the elasto-plastic-viscoplastic rock mass (EPVP) with viscoelastic lining (VEL) (dotted lines) shows superior convergences compared to the elastoplastic (EP) model with elastic lining (EL) (solid lines). Because the young age of the viscoelastic lining (VEL) has a lower modulus of elasticity, resulting in lower stiffness. Therefore, compared to the elastic lining (EL), the lower initial value of the modulus of elasticity contributes more to the development of convergence. In the long term (LT), even though the viscoelastic lining (VEL) (dashed lines) has a higher stiffness due to a aging of lining, the viscous effects over time result in a significantly more discrepant convergence profile compared to the elastoplastic model (EP) with elastic lining (EL) (solid lines). There is a noticeable increase in the magnitude of U_{peak} between the short term and the long term at the gallery position, highlighting the influence of the viscoelastic lining.

To study the effect of the lining, Fig. 22 and 23 show the elastoplastic rock mass (EP) under various conditions: without lining (NL), with a moderately stiff elastic lining ($K_c = 1027$ MPa), and with a highly stiff lining ($K_c = 3660$ MPa) with (WG) and without gallary (NG).

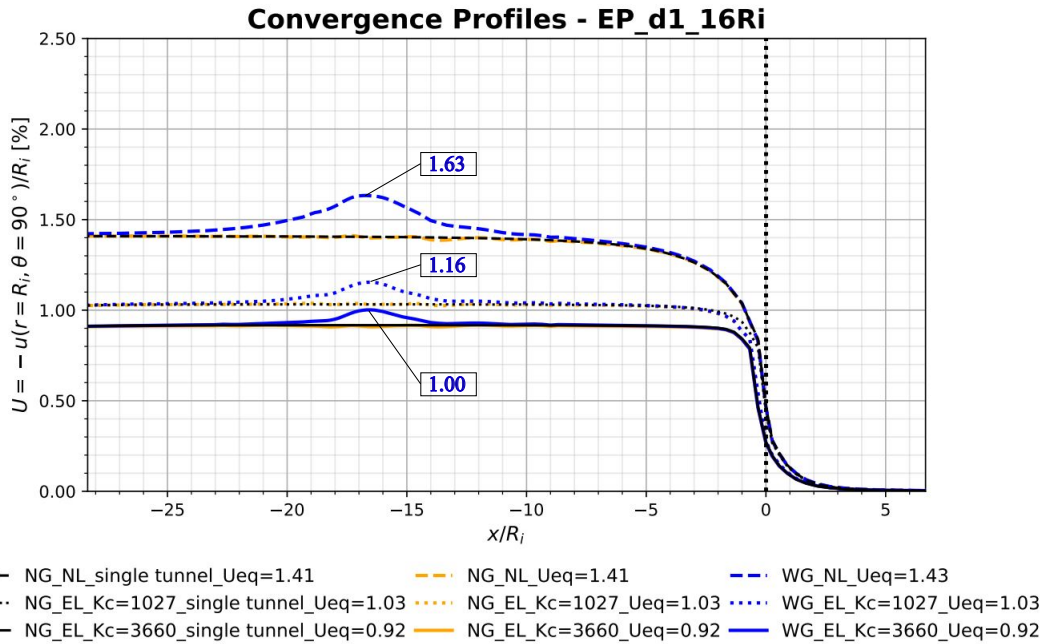


Figure 22: Convergence Profiles - elastoplastic rock mass (EP) without lining (NL) with a highly stiff elastic lining ($K_c = 3660$ MPa) and a moderately stiff elastic lining ($K_c = 1027$ MPa), without (NG) and with gallery (WG) for $d_1 = 16R_i$

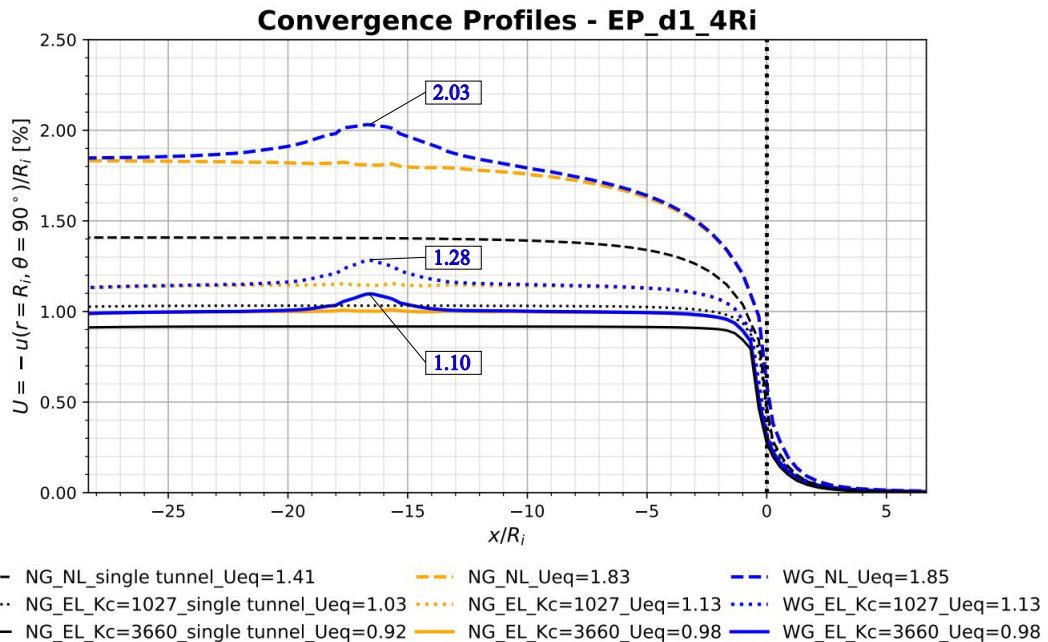


Figure 23: Convergence Profiles - elastoplastic rock mass (EP) without lining (NL) with a highly stiff elastic lining ($K_c = 3660$ MPa) and a moderately stiff elastic lining ($K_c = 1027$ MPa), without (NG) and with gallery (WG) for $d_1 = 4R_i$

For the single tunnel, a high stiffness lining (black solid line) decreases convergence by approximately 35% compared to the unlined model (black dashed line). Conversely, a moderately stiff lining (black dotted line) increases convergence by 12% compared to the rigid lining.

When $d_1 = 16R_i$ between the twin tunnels (blue and yellow lines), the results of U_{eq} are similar to the isolated tunnel (black line). However, with a distance reduced to $d_1 = 4R_i$, the interaction between the tunnels becomes significant. A smaller d_1 , the high stiffness lining (solid yellow and blue lines) can restrict convergence by up to 46% of the unlined (dashed yellow and blue lines) convergence. A moderate stiffness lining (dotted lines) leads to an increase of up to 16% in convergence compared to the high stiffness lining (solid lines).

When comparing results between twin lined tunnels with spacings of $16R_i$ and $4R_i$, differences of 6% with high stiffness lining (solid yellow and blue lines), 10% with moderate stiffness lining (dotted yellow and blue lines), and 30% without lining (dashed yellow and blue lines) are observed. These results show the direct impact of lining stiffness and the distance between twin tunnels on U_{eq} convergence.

When analyzing the convergence U_{peak} at the point where the gallery meets the longitudinal tunnel, there is an increase of 16% when using a moderate stiffness elastic lining (dotted blue line) compared to a high stiffness lining (solid blue line). However, when analyzing the difference between the U_{eq} and U_{peak} , there is a difference of up to 12% for the high stiffness elastic lining (solid blue line to $4R_i$ and $16R_i$) and up to 13% for the moderate stiffness elastic lining (dotted blue line to $4R_i$ and $16R_i$) for $d_1 = 4R_i$.

Applying the same type of previously analysis, we examine the elasto-plastic-viscoplastic model for the rock mass (EPVP), considering the presence of a viscoelastic lining (VEL) (Figs. 24 and 25). This analysis aims to comprehend the influence of the lining's stiffness, particularly when the twin tunnels are nearby. The results reveal that, once again, the convergence profile under these conditions, with a distance of $16R_i$ between the tunnels, closely resembles that of an isolated tunnel. Differences are on the order of 1.8% for a moderately stiff lining and 0.8% for a highly stiff lining.

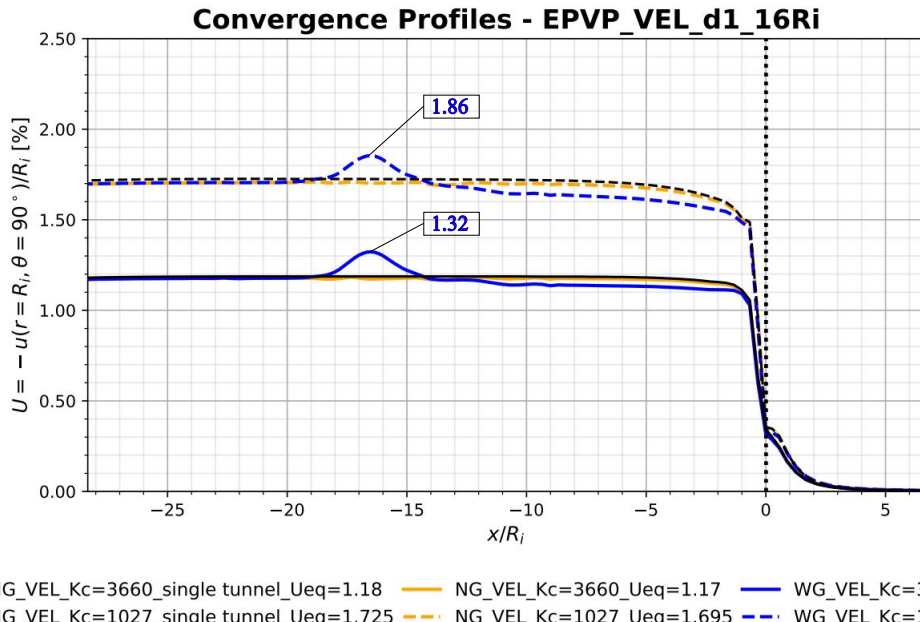


Figure 24: Convergence Profiles - elasto-plastic-viscoplastic rock mass (EPVP) with a highly stiff viscoelastic lining ($K_c = 3660$ MPa) and a moderately stiff viscoelastic lining ($K_c = 1027$ MPa), without (NG) and with gallery (WG) for $d_1 = 16R_i$

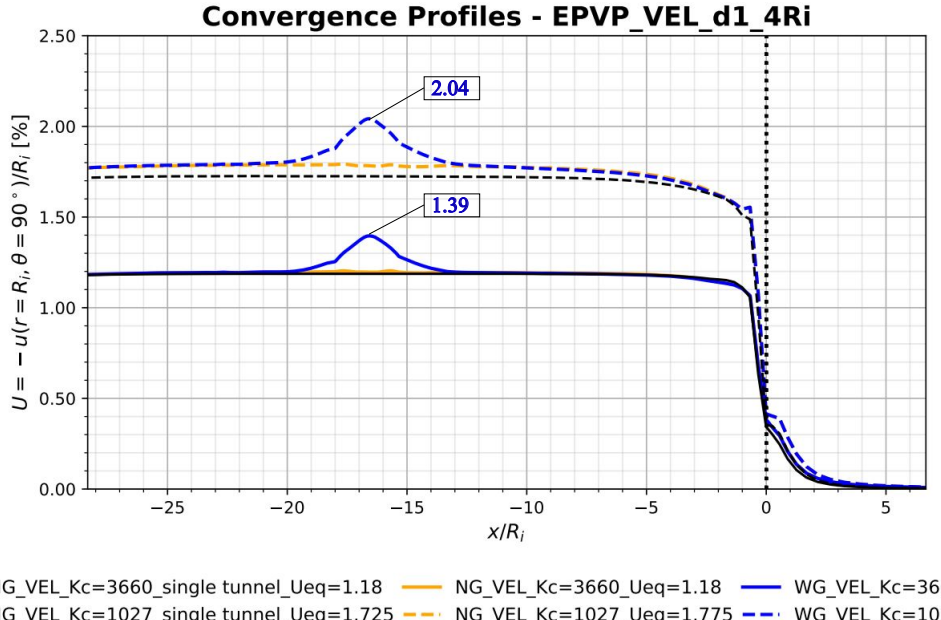


Figure 25: Convergence Profiles - elasto-plastic-viscoplastic rock mass (EPVP) with a highly stiff viscoelastic lining ($K_c = 3660$ MPa) and a moderately stiff viscoelastic lining ($K_c = 1027$ MPa), without (NG) and with gallery (WG) for $d_1 = 4R_i$

In the case of $d_1 = 4R_i$, when a high stiffness lining is applied (blue and yellow solid lines), there is practically no difference compared to the isolated tunnel (black solid line). This occurs because the high rigidity of the lining blocks convergence in the interaction between the tunnels. However, when using a moderately stiff lining (blue and yellow dashed lines), there is a difference of approximately 3% in the convergence U_{eq} compared to the single tunnel (black dashed line).

When comparing the results for $d_1 = 16R_i$ and $4R_i$, considering each lining separately, there is a difference of 0.8% when there is a high stiffness lining (solid yellow and blue lines to $16R_i$ and $4R_i$) and 4.8% for a moderate stiffness lining (dashed yellow and blue lines to $16R_i$ and $4R_i$). Thus, once again, the importance of the stiffness of the lining when associated with the distance between the twin tunnels.

When analyzing the convergence U_{peak} at the point where the gallery meets the longitudinal tunnel, there is an increase of 47% for $d_1 = 4R_i$ when using a moderate stiffness lining (dashed blue line) compared to a high stiffness lining (solid blue line). However, when analyzing the difference between the U_{eq} and U_{peak} , there is a difference of up to 18% for the high stiffness elastic lining (solid blue line) and up to 15% for the moderate stiffness lining (dashed blue line) for $d_1 = 4R_i$.

The following results (Figs. 26 and 27) compare the elastic (EL) and viscoelastic (VEL) lining with high and moderate stiffness, considering the elastoplastic-viscoplastic (EPVP) model for the rock mass.

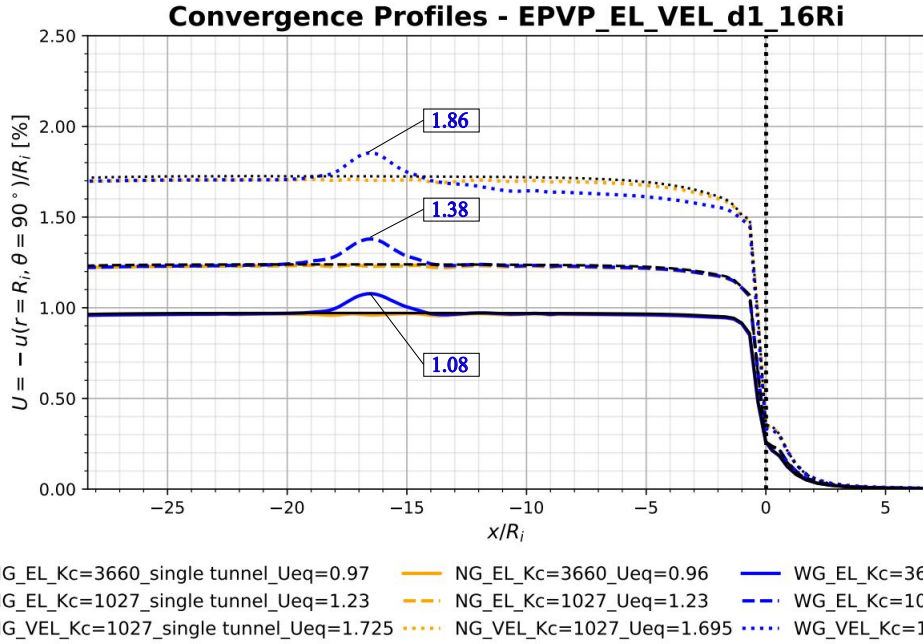


Figure 26: Convergence Profiles - elasto-plastic-viscoplastic rock mass (EPVP) without lining (NL) with a highly stiff ($K_c = 3660$ MPa) and a moderately stiff ($K_c = 1027$ MPa) elastic (EL) and viscoelastic (VEL) lining, without (NG) and with gallery (WG) for $d_1 = 16R_i$

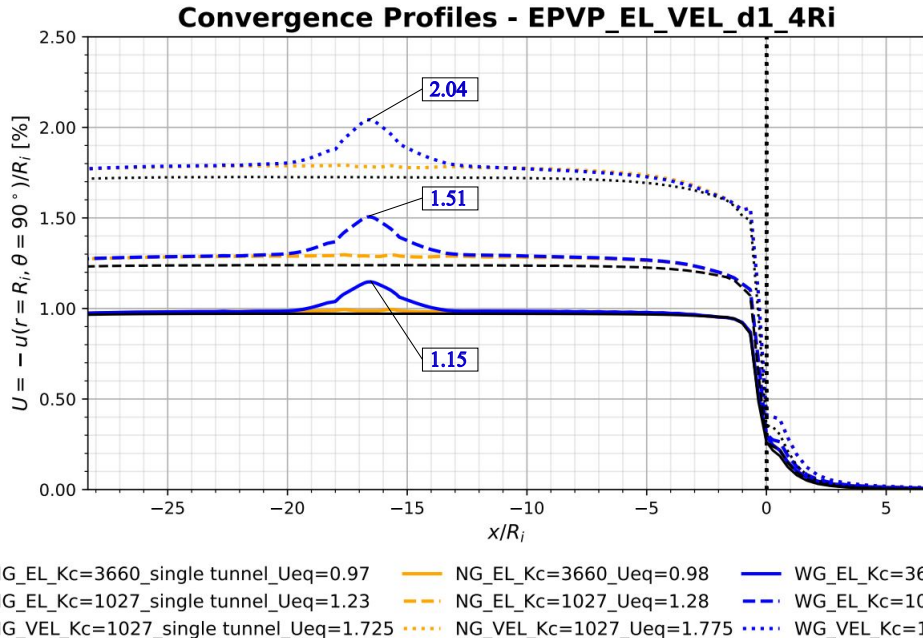


Figure 27: Convergence Profiles - elasto-plastic-viscoplastic rock mass (EPVP) without lining (NL) with a highly stiff ($K_c = 3660$ MPa) and a moderately stiff ($K_c = 1027$ MPa) elastic (EL) and viscoelastic (VEL) lining, without (NG) and with gallery (WG) for $d_1 = 4R_i$

For $d_1 = 16R_i$, the significant difference in U_{eq} compared to the isolated tunnel (dotted black line) occurs when considering the moderate stiffness viscoelastic lining (dotted blue line), with approximately 1.8%. In contrast, for $d_1 = 4R_i$, the differences are 4% and 3% for the elastic (dashed lines) and viscoelastic (dotted lines) linings with moderate stiffness, respectively.

When adopting the high stiffness elastic lining as a reference (solid lines), for $d_1 = 16R_i$, the differences increase to 27% and 78% when comparing the elastic (dashed lines) and viscoelastic (dotted lines) lining with moderate stiffness, respectively, and to 31% and 81% in the case of $d_1 = 4R_i$.

When analyzing the convergence at the peak U_{peak} , which corresponds to the point where the gallery meets the longitudinal tunnel, and using the value of the high stiffness elastic lining (solid lines) as the reference, an increase of up to 31% and 77% is observed for $d_1 = 4R_i$ when using the elastic (dashed lines) and viscoelastic (dotted lines) linings of moderate stiffness, respectively.

However, when analyzing the difference between the U_{eq} and U_{peak} , there is a difference of up to 18% for the moderate stiffness elastic lining (dashed blue line) and up to 15% for the moderate stiffness viscoelastic lining (dotted blue line) for $d_1 = 4R_i$.

Finally, Fig. 28 a comparison between the lining elastic and viscoelastic, considering high and moderate stiffness, and between the elastoplastic and elastoplastic-viscoplastic models for the rock mass. We adopt the condition of an isolated tunnel, starting from the reference value of the elastoplastic rock mass with high stiffness elastic lining.

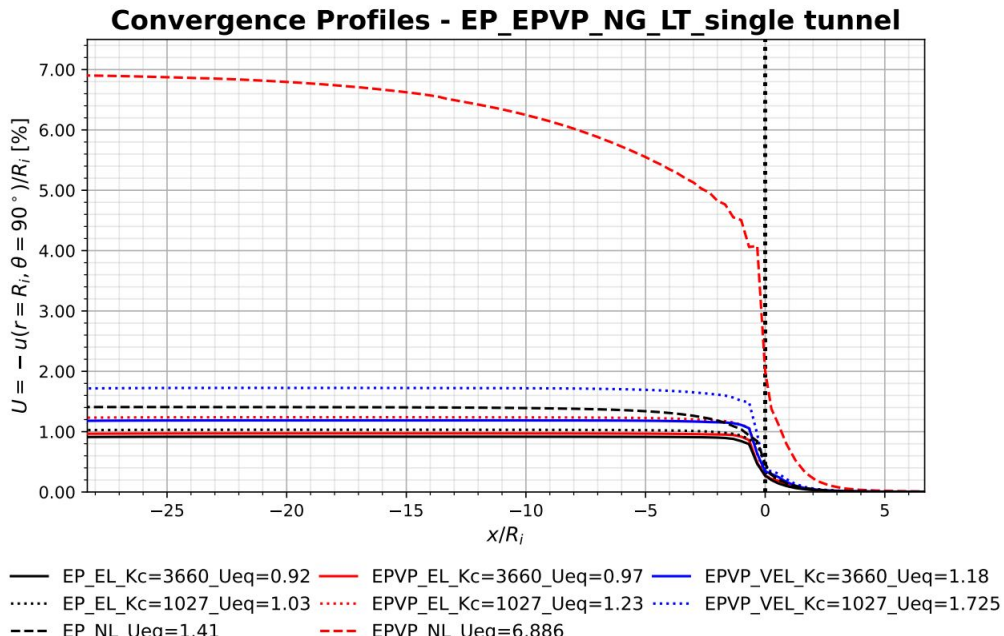


Figure 28: Convergence Profiles – single tunnel with elastoplastic (EP) and elasto-plastic-viscoplastic rock mass (EPVP), without lining (NL) with a highly stiff ($K_c = 3660$ MPa) and a moderately stiff ($K_c = 1027$ MPa) elastic (EL) and viscoelastic (VEL) lining

Taking as a reference the elastoplastic model with a highly stiffness elastic lining (solid black line) we observed a difference of 12% and 53.5%, respectively, in the cases of the elastoplastic rock mass with an elastic lining of moderate stiffness (dotted black) and without a lining (dashed black line). We also identified a difference of 5.5%, 33.5%, and 748% when using the elastoplastic-viscoplastic model for the rock mass with an elastic lining of high stiffness (solid red line), moderate stiffness (dotted red line), and no lining (dashed red line). In addition, we found a difference of 28% and 87.5% when comparing the elastoplastic-viscoplastic model for the rock mass and the viscoelastic model for the high stiffness (solid blue line) and moderate stiffness lining (dotted blue line), respectively.

8. Conclusions

The fundamental role of the stiffness of the concrete lining in the convergence profile of twin tunnels is understood from the analyses. Depending on the value of this stiffness, it is possible to condition the restriction of viscous effects that tend to manifest over time after the completion of the excavation process.

Additionally, the effect of the interaction between longitudinal tunnels is notable when considering proximity, with significant influence from a distance of 4 radii. However, in many cases, this effect may be subtle or almost imperceptible due to the presence of a highly rigid lining.

In models considering the viscosity of the rock mass, the time factor plays a significant role in convergence. In this scenario, when excavating the gallery with $d_1 = 16R_i$, the portion of the tunnel already excavated remains subject to viscous effects for a more extended period compared to other distances. In any case, when $d_1 = 4R_i$, the proximity interaction between twin tunnels, along with viscous effects over time, results in a higher value compared to cases where $d_1 = 16R_i$ and $8R_i$.

Another important observation related to EPVP-EL and EPVP-VEL models concerns the possible ovalization of the section over time, concerning the analyzed reference point on the section perimeter (in the crown). Instead of following the logic of following the closing direction of the section, it may undergo some negative displacement in the long term. The result, for the same observation point, is a convergence value that in the short term may indicate section closure but in the long term may indicate the opposite.

Another crucial observation regarding EPVP-EL and EPVP-VEL models pertains to the potential ovalization of the section over time, particularly concerning the analyzed reference point on the section perimeter (in the crown). Instead of conforming to the expected logic of closing in the section's direction, it might experience negative displacement in the long term. Consequently, for the same observation point, the convergence value may initially suggest section closure in the short-term but indicate the opposite in the long-term.

Concerning the EPVP-VEL model, specifically with distances of 16 and 8 radii between twin tunnels, we observe that U_{eq} in the section ahead of the gallery region is slightly smaller than U_{eq} in the section preceding the gallery. This variation in the convergence profile results from the shorter exposure time to viscous effects in the portion excavated later than the transverse gallery. Therefore, during the gallery excavation process, the portion of the longitudinal tunnel already excavated experiences viscous effects until completing the gallery excavation.

However, concerning the existence of a transverse gallery and adopting the constitutive parameters while considering the presence of lining, its influence is highly localized, spanning approximately four radii on each side from its axis. Consequently, there is no significant impact on the remaining convergence profile of the tunnels, except for the model with viscoelastic lining, where lower convergences occur after the gallery.

References

- ANSYS, 2013. ANSYS Programmer's Reference; release 15.0. Canonsburg, Pennsylvania.
- Bažant, Z.P., Prasannan, S., 1989a. Solidification theory for concrete creep. i: Formulation. *Journal of engineering mechanics* 115, 1691–1703. doi:[https://doi.org/10.1061/\(ASCE\)0733-9399\(1989\)115:8\(1691\)](https://doi.org/10.1061/(ASCE)0733-9399(1989)115:8(1691)).
- Bažant, Z.P., Prasannan, S., 1989b. Solidification theory for concrete creep. ii: Verification and application. *Journal of engineering mechanics* 115, 1704–1725. doi:[https://doi.org/10.1061/\(ASCE\)0733-9399\(1989\)115:8\(1704\)](https://doi.org/10.1061/(ASCE)0733-9399(1989)115:8(1704)).
- Bernaud, D., 1991. Tunnels profonds dans les milieux viscoplastiques: approches expérimentale et numérique. Ph.D. thesis. Ecole Nationale des Ponts et Chaussées. Paris, French. URL: <https://theses.hal.science/tel-00529719/>.
- CEB-FIP, 1993. CEB-FIP model code 1990: Design code. Comité Euro International du Béton and Fédération Internationale de la Précontrainte (CEB-FIP).
- Chen, F., Lin, L.b., Li, D., 2019. Analytic solutions for twin tunneling at great depth considering liner installation and mutual interaction between geomaterial and liners. *Applied Mathematical Modelling* 73. doi:10.1016/j.apm.2019.04.026.
- Chortis, F., Kavvadas, M., 2021a. Three-dimensional numerical analyses of perpendicular tunnel intersections. *Geotechnical and Geological Engineering* 39, 1771–1793.
- Chortis, F., Kavvadas, M., 2021b. Three-dimensional numerical investigation of the interaction between twin tunnels. *Geotechnical and Geological Engineering* 39, 5559–5585. doi:<https://doi.org/10.1007/s10706-021-01845-5>.
- Chortis, F., Kavvadas, M., 2023a. 3d numerical investigation of the axial forces acting on tunnel junctions constructed in fractured/weathered to very blocky rockmass, in: Expanding Underground-Knowledge and Passion to Make a Positive Impact on the World. CRC Press, pp. 1574–1582.
- Chortis, F., Kavvadas, M., 2023b. 3d numerical investigation of the bending moments acting on tunnel junctions constructed in fractured/weathered to very blocky rockmass, in: Expanding Underground-Knowledge and Passion to Make a Positive Impact on the World. CRC Press, pp. 1583–1591.
- Fortsakis, P., Bekri, E., Prountzopoulos, G., Marinos, P., 2012. Numerical analysis of twin tunnels interaction, in: in Proc. 1st Eastern European Tunnelling Conference, pp. 1–8.

- Guo, Z., Liu, X., Zhu, Z., 2021. An elastic solution for twin circular tunnels' stress in hydrostatic stress field. *Geotechnical and Geological Engineering* 39, 1–11. doi:10.1007/s10706-021-01756-5.
- Ma, Y., Lu, A., Zeng, X., Cai, H., 2020. Analytical solution for determining the plastic zones around twin circular tunnels excavated at great depth. *International Journal of Rock Mechanics and Mining Sciences* 136, 104475. doi:<https://doi.org/10.1016/j.ijrmms.2020.104475>.
- Piepi, G.T., 1995. Comportement viscoplastique avec rupture des argiles raides. Applications aux ouvrages souterrains. Ph.D. thesis. Ecole Nationale des Ponts et Chaussées. Paris, French. URL: <https://pastel.hal.science/tel-00523616/document>.
- Quevedo, F.P.M., 2017. Comportamento a longo prazo de túneis profundos revestidos com concreto: modelo em elementos finitos. M.S. thesis. Federal University of Rio Grande do Sul. Porto Alegre, Brazil. URL: <https://lume.ufrgs.br/handle/10183/163886>.
- Quevedo, F.P.M., 2021. Análise computacional das deformações em túneis profundos considerando o acoplamento plasticidade-viscoplasticidade. URL: <https://lume.ufrgs.br/handle/10183/239617>.
- Quevedo, F.P.M., Bernaud, D., Campos Filho, A., 2022a. Numerical analysis of deep tunnels in viscoplastic rock mass considering the creep and shrinkage of the concrete lining. *International Journal of Geomechanics* 22. doi:10.1061/(ASCE)GM.1943-5622.0002282.
- Quevedo, F.P.M., Bernaud, D., S., M., 2022b. Numerical integration scheme for coupled elastoplastic–viscoplastic constitutive law for tunnels. *International Journal of Geomechanics* 22. doi:10.1061/(ASCE)GM.1943-5622.0002512.
- Spyridis, P., Bergmeister, K., 2015. Analysis of lateral openings in tunnel linings. *Tunnelling and Underground Space Technology* 50, 376–395. doi:10.1016/j.tust.2015.08.005.
- Zienkiewicz, O., Cormeau, I., 1974. Visco-plasticity—plasticity and creep in elastic solids—a unified numerical solution approach. *International Journal for Numerical Methods in Engineering* 8, 821–845. doi:<https://doi.org/10.1002/nme.v8:4>.

```
This is pdfTeX, Version 3.141592653-2.6-1.40.24 (TeX Live 2022)
(preloaded format=pdflatex 2023.3.8) 2 DEC 2023 22:16
entering extended mode
  restricted \write18 enabled.
  %&-line parsing enabled.
**cas-dc-template.tex
./cas-dc-template.tex
TeXLive <2022-11-01> patch level 1
L3 programming layer <2023-02-22> ./cas-dc.cls
Document Class: cas-dc 2021/05/11, 2.3: Formatting class for CAS double
column
articles
\c@blind=\count185
\@bls=\dimen140
(c:/TeXLive/2022/texmf-dist/tex/latex/base/article.cls
Document Class: article 2022/07/02 v1.4n Standard LaTeX document class
(c:/TeXLive/2022/texmf-dist/tex/latex/base/fleqn.clo
File: fleqn.clo 2016/12/29 v1.2b Standard LaTeX option (flush left
equations)
\mathindent=\skip48
Applying: [2015/01/01] Make \[ robust on input line 50.
TeX Info: Redefining \[ on input line 51.
Already applied: [0000/00/00] Make \[ robust on input line 62.
Applying: [2015/01/01] Make \] robust on input line 74.
TeX Info: Redefining \] on input line 75.
Already applied: [0000/00/00] Make \] robust on input line 83.
) (c:/TeXLive/2022/texmf-dist/tex/latex/base/size10.clo
File: size10.clo 2022/07/02 v1.4n Standard LaTeX file (size option)
)
\c@part=\count186
\c@section=\count187
\c@subsection=\count188
\c@subsubsection=\count189
\c@paragraph=\count190
\c@ subparagraph=\count191
\c@figure=\count192
\c@table=\count193
\abovecaptionskip=\skip49
\belowcaptionskip=\skip50
\bibindent=\dimen141
) (c:/TeXLive/2022/texmf-dist/tex/latex/graphics/graphicx.sty
Package: graphicx 2021/09/16 v1.2d Enhanced LaTeX Graphics (DPC,SPQR)
(c:/TeXLive/2022/texmf-dist/tex/latex/graphics/keyval.sty
Package: keyval 2022/05/29 v1.15 key=value parser (DPC)
\KV@toks@=\toks16
) (c:/TeXLive/2022/texmf-dist/tex/latex/graphics/graphics.sty
Package: graphics 2022/03/10 v1.4e Standard LaTeX Graphics (DPC,SPQR)
(c:/TeXLive/2022/texmf-dist/tex/latex/graphics/trig.sty
Package: trig 2021/08/11 v1.11 sin cos tan (DPC)
) (c:/TeXLive/2022/texmf-dist/tex/latex/graphics-cfg/graphics.cfg
File: graphics.cfg 2016/06/04 v1.11 sample graphics configuration
)
Package graphics Info: Driver file: pdftex.def on input line 107.
(c:/TeXLive/2022/texmf-dist/tex/latex/graphics-def/pdftex.def
```

```
File: pdftex.def 2022/09/22 v1.2b Graphics/color driver for pdftex
))
\Gin@req@height=\dimen142
\Gin@req@width=\dimen143
) (c:/TeXLive/2022/texmf-dist/tex/latex/amsmath/amsmath.sty
Package: amsmath 2022/04/08 v2.17n AMS math features
\@mathmargin=\skip51
For additional information on amsmath, use the `?' option.
(c:/TeXLive/2022/texmf-dist/tex/latex/amsmath/amstext.sty
Package: amstext 2021/08/26 v2.01 AMS text
(c:/TeXLive/2022/texmf-dist/tex/latex/amsmath/amsgen.sty
File: amsgen.sty 1999/11/30 v2.0 generic functions
\@emptytoks=\toks17
\ex@=\dimen144
)) (c:/TeXLive/2022/texmf-dist/tex/latex/amsmath/amsbsy.sty
Package: amsbsy 1999/11/29 v1.2d Bold Symbols
\pmbraise@=\dimen145
) (c:/TeXLive/2022/texmf-dist/tex/latex/amsmath/amsopn.sty
Package: amsopn 2022/04/08 v2.04 operator names
)
\inf@bad=\count194
LaTeX Info: Redefining \frac on input line 234.
\uproot@=\count195
\leftroot@=\count196
LaTeX Info: Redefining \overline on input line 399.
LaTeX Info: Redefining \colon on input line 410.
\classnum@=\count197
\DOTSCASE@=\count198
LaTeX Info: Redefining \ldots on input line 496.
LaTeX Info: Redefining \dots on input line 499.
LaTeX Info: Redefining \cdots on input line 620.
\Mathstrutbox@=\box51
\strutbox@=\box52
LaTeX Info: Redefining \big on input line 722.
LaTeX Info: Redefining \Big on input line 723.
LaTeX Info: Redefining \bigg on input line 724.
LaTeX Info: Redefining \Bigg on input line 725.
\big@size=\dimen146
LaTeX Font Info:     Redeclaring font encoding OML on input line 743.
LaTeX Font Info:     Redeclaring font encoding OMS on input line 744.
\macc@depth=\count199
LaTeX Info: Redefining \bmod on input line 905.
LaTeX Info: Redefining \pmod on input line 910.
LaTeX Info: Redefining \smash on input line 940.
LaTeX Info: Redefining \relbar on input line 970.
LaTeX Info: Redefining \Relbar on input line 971.
\c@MaxMatrixCols=\count266
\dotsspace@=\muskip16
\c@parentequation=\count267
\dspbrk@lvl=\count268
\tag@help=\toks18
\row@=\count269
\column@=\count270
\maxfields@=\count271
```

```
\andhelp@=\toks19
\eqnshift@=\dimen147
\alignsep@=\dimen148
\tagshift@=\dimen149
\tagwidth@=\dimen150
\totwidth@=\dimen151
\lineht@=\dimen152
@envbody=\toks20
\multlinegap=\skip52
\multlinetaggap=\skip53
\mathdisplay@stack=\toks21
LaTeX Info: Redefining \[ on input line 2953.
LaTeX Info: Redefining \] on input line 2954.
) (c:/TeXLive/2022/texmf-dist/tex/latex/amsfonts/amsfonts.sty
Package: amsfonts 2013/01/14 v3.01 Basic AMSFonts support
\symAMSA=\mathgroup4
\symAMSB=\mathgroup5
LaTeX Font Info: Redeclaring math symbol \hbar on input line 98.
LaTeX Font Info: Overwriting math alphabet `mathfrak' in version
`bold'
(Font)           U/euf/m/n --> U/euf/b/n on input line 106.
) (c:/TeXLive/2022/texmf-dist/tex/latex/amsfonts/amssymb.sty
Package: amssymb 2013/01/14 v3.01 AMS font symbols
) (c:/TeXLive/2022/texmf-dist/tex/latex/l3kernel/expl3.sty
Package: expl3 2023-02-22 L3 programming layer (loader)
(c:/TeXLive/2022/texmf-dist/tex/latex/l3backend/l3backend-pdfTeX.def
File: l3backend-pdfTeX.def 2023-01-16 L3 backend support: PDF output
(pdfTeX)
\l_color_backend_stack_int=\count272
\l_pdf_internal_box=\box53
)) (c:/TeXLive/2022/texmf-dist/tex/latex/l3packages/xparse/xparse.sty
Package: xparse 2023-02-02 L3 Experimental document command parser
) (c:/TeXLive/2022/texmf-dist/tex/latex/etoolbox/etoolbox.sty
Package: etoolbox 2020/10/05 v2.5k e-TeX tools for LaTeX (JAW)
\etb@tempcnta=\count273
) (c:/TeXLive/2022/texmf-dist/tex/latex/preprint/balance.sty
Package: balance 1999/02/23 4.3 (PWD)
\oldvsize=\dimen153
) (c:/TeXLive/2022/texmf-dist/tex/latex/booktabs/booktabs.sty
Package: booktabs 2020/01/12 v1.61803398 Publication quality tables
\heavyrulewidth=\dimen154
\lightrulewidth=\dimen155
\cmidrulewidth=\dimen156
\belowrulesep=\dimen157
\belowbottomsep=\dimen158
\aboverulesep=\dimen159
\abovetopsep=\dimen160
\cmidrulesep=\dimen161
\cmidrulekern=\dimen162
\defaultaddspace=\dimen163
@cmidla=\count274
@cmidlb=\count275
@aboverulesep=\dimen164
@belowrulesep=\dimen165
```

```
\@thisruleclass=\count276
\@lastruleclass=\count277
\@thisrulewidth=\dimen166
) (c:/TeXLive/2022/texmf-dist/tex/latex/makecell/makecell.sty
Package: makecell 2009/08/03 V0.1e Managing of Tab Column Heads and Cells
(c:/TeXLive/2022/texmf-dist/tex/latex/tools/array.sty
Package: array 2022/09/04 v2.5g Tabular extension package (FMi)
\col@sep=\dimen167
\ar@mcellbox=\box54
\extrarowheight=\dimen168
\NC@list=\toks22
\extratabsurround=\skip54
\backup@length=\skip55
\ar@cellbox=\box55
)
\rotheadsize=\dimen169
\c@nlinenum=\count278
\TeXr@lab=\toks23
) (c:/TeXLive/2022/texmf-dist/tex/latex/multirow/multirow.sty
Package: multirow 2021/03/15 v2.8 Span multiple rows of a table
\multirow@colwidth=\skip56
\multirow@cntb=\count279
\multirow@dima=\skip57
\bigstrutjot=\dimen170
) (c:/TeXLive/2022/texmf-dist/tex/latex/coltbl/coltbl.sty
Package: coltbl 2022/06/20 v1.0f Color table columns (DPC)
(c:/TeXLive/2022/texmf-dist/tex/latex/graphics/color.sty
Package: color 2022/01/06 v1.3d Standard LaTeX Color (DPC)
(c:/TeXLive/2022/texmf-dist/tex/latex/graphics-cfg/color.cfg
File: color.cfg 2016/01/02 v1.6 sample color configuration
)
Package color Info: Driver file: pdftex.def on input line 149.
(c:/TeXLive/2022/texmf-dist/tex/latex/mathcolor.ltx))
\everycr=\toks24
\minrowclearance=\skip58
\rownum=\count280
) (c:/TeXLive/2022/texmf-dist/tex/tools/dcolumn.sty
Package: dcolumn 2014/10/28 v1.06 decimal alignment package (DPC)
) (c:/TeXLive/2022/texmf-dist/tex/latex/stftools/stffloats.sty
Package: stffloats 2017/03/27 v3.3 Improve float mechanism and
baselineskip sett
ings
\@dblbotnum=\count281
\c@dblbotnumber=\count282
) (c:/TeXLive/2022/texmf-dist/tex/tools/xspace.sty
Package: xspace 2014/10/28 v1.13 Space after command names (DPC,MH)
) (c:/TeXLive/2022/texmf-dist/tex/generic/xstring/xstring.sty
(c:/TeXLive/2022/
texmf-dist/tex/generic/xstring/xstring.tex
\integerpart=\count283
\decimalpart=\count284
)
Package: xstring 2023/01/14 v1.85 String manipulations (CT)
) (c:/TeXLive/2022/texmf-dist/tex/latex/footmisc/footmisc.sty
```

```
Package: footmisc 2022/03/08 v6.0d a miscellany of footnote facilities
\FN@temptoken=\toks25
\footnotemargin=\dimen171
\@outputbox@depth=\dimen172
Package footmisc Info: Declaring symbol style bringhurst on input line
695.
Package footmisc Info: Declaring symbol style chicago on input line 703.
Package footmisc Info: Declaring symbol style wiley on input line 712.
Package footmisc Info: Declaring symbol style lampert-robust on input
line 723.

Package footmisc Info: Declaring symbol style lamport* on input line 743.
Package footmisc Info: Declaring symbol style lamport*-robust on input
line 764
.
) (c:/TeXLive/2022/texmf-dist/tex/latex/xcolor/xcolor.sty
Package: xcolor 2022/06/12 v2.14 LaTeX color extensions (UK)
(c:/TeXLive/2022/texmf-dist/tex/latex/graphics-cfg/color.cfg
File: color.cfg 2016/01/02 v1.6 sample color configuration
)
Package xcolor Info: Driver file: pdftex.def on input line 227.
LaTeX Info: Redefining \color on input line 711.
(c:/TeXLive/2022/texmf-dist/tex/latex/mathcolor.ltx)
Package xcolor Info: Model `cmy' substituted by `cmy0' on input line
1353.
Package xcolor Info: Model `hsb' substituted by `rgb' on input line 1357.
Package xcolor Info: Model `RGB' extended on input line 1369.
Package xcolor Info: Model `HTML' substituted by `rgb' on input line
1371.
Package xcolor Info: Model `Hsb' substituted by `hsb' on input line 1372.
Package xcolor Info: Model `tHsb' substituted by `hsb' on input line
1373.
Package xcolor Info: Model `HSB' substituted by `hsb' on input line 1374.
Package xcolor Info: Model `Gray' substituted by `gray' on input line
1375.
Package xcolor Info: Model `wave' substituted by `hsb' on input line
1376.
(c:/TeXLive/2022/texmf-dist/tex/graphics/dvipsnam.def
File: dvipsnam.def 2016/06/17 v3.0m Driver-dependent file (DPC,SPQR)
) (c:/TeXLive/2022/texmf-dist/tex/latex/xcolor/svgnam.def
File: svgnam.def 2022/06/12 v2.14 Predefined colors according to SVG 1.1
(UK)
)) (c:/TeXLive/2022/texmf-dist/tex/latex/hyperref/hyperref.sty
Package: hyperref 2023-02-07 v7.00v Hypertext links for LaTeX
(c:/TeXLive/2022/texmf-dist/tex/generic/ltxcmds/ltxcmds.sty
Package: ltxcmds 2020-05-10 v1.25 LaTeX kernel commands for general use
(HO)
) (c:/TeXLive/2022/texmf-dist/tex/generic/iftex/iftex.sty
Package: iftex 2022/02/03 v1.0f TeX engine tests
) (c:/TeXLive/2022/texmf-dist/tex/generic/pdftexcmds/pdftexcmds.sty
Package: pdftexcmds 2020-06-27 v0.33 Utility functions of pdfTeX for
LuaTeX (HO
)
(c:/TeXLive/2022/texmf-dist/tex/generic/infwarerr/infwarerr.sty
```

```
Package: infwarerr 2019/12/03 v1.5 Providing info/warning/error messages
(HO)
)
Package pdftexcmds Info: \pdf@primitive is available.
Package pdftexcmds Info: \pdf@ifprimitive is available.
Package pdftexcmds Info: \pdfdraftmode found.
) (c:/TeXLive/2022/texmf-dist/tex/latex/kvsetkeys/kvsetkeys.sty
Package: kvsetkeys 2022-10-05 v1.19 Key value parser (HO)
) (c:/TeXLive/2022/texmf-dist/tex/generic/kvdefinekeys/kvdefinekeys.sty
Package: kvdefinekeys 2019-12-19 v1.6 Define keys (HO)
) (c:/TeXLive/2022/texmf-dist/tex/generic/pdfescape/pdfescape.sty
Package: pdfescape 2019/12/09 v1.15 Implements pdfTeX's escape features
(HO)
) (c:/TeXLive/2022/texmf-dist/tex/latex/hycolor/hycolor.sty
Package: hycolor 2020-01-27 v1.10 Color options for hyperref/bookmark
(HO)
) (c:/TeXLive/2022/texmf-dist/tex/latex/letltxmacro/letltxmacro.sty
Package: letltxmacro 2019/12/03 v1.6 Let assignment for LaTeX macros (HO)
) (c:/TeXLive/2022/texmf-dist/tex/latex/auxhook/auxhook.sty
Package: auxhook 2019-12-17 v1.6 Hooks for auxiliary files (HO)
) (c:/TeXLive/2022/texmf-dist/tex/latex/hyperref/nameref.sty
Package: nameref 2022-05-17 v2.50 Cross-referencing by name of section
(c:/TeXLive/2022/texmf-dist/tex/latex/refcount/refcount.sty
Package: refcount 2019/12/15 v3.6 Data extraction from label references
(HO)
) (c:/TeXLive/2022/texmf-
dist/tex/generic/gettitlestring/gettitlestring.sty
Package: gettitlestring 2019/12/15 v1.6 Cleanup title references (HO)
(c:/TeXLive/2022/texmf-dist/tex/latex/kvoptions/kvoptions.sty
Package: kvoptions 2022-06-15 v3.15 Key value format for package options
(HO)
))
\c@section@level=\count285
)
\@linkdim=\dimen173
\Hy@linkcounter=\count286
\Hy@pagecounter=\count287
(c:/TeXLive/2022/texmf-dist/tex/latex/hyperref/pd1enc.def
File: pd1enc.def 2023-02-07 v7.00v Hyperref: PDFDocEncoding definition
(HO)
Now handling font encoding PD1 ...
... no UTF-8 mapping file for font encoding PD1
) (c:/TeXLive/2022/texmf-dist/tex/generic/intcalc/intcalc.sty
Package: intcalc 2019/12/15 v1.3 Expandable calculations with integers
(HO)
) (c:/TeXLive/2022/texmf-dist/tex/generic/etexcmds/etexcmds.sty
Package: etexcmds 2019/12/15 v1.7 Avoid name clashes with e-TeX commands
(HO)
)
\Hy@SavedSpaceFactor=\count288
(c:/TeXLive/2022/texmf-dist/tex/latex/hyperref/puenc.def
File: puenc.def 2023-02-07 v7.00v Hyperref: PDF Unicode definition (HO)
Now handling font encoding PU ...
... no UTF-8 mapping file for font encoding PU
```

```
)  
Package hyperref Info: Option `colorlinks' set `true' on input line 4060.  
Package hyperref Info: Hyper figures OFF on input line 4177.  
Package hyperref Info: Link nesting OFF on input line 4182.  
Package hyperref Info: Hyper index ON on input line 4185.  
Package hyperref Info: Plain pages OFF on input line 4192.  
Package hyperref Info: Backreferencing OFF on input line 4197.  
Package hyperref Info: Implicit mode ON; LaTeX internals redefined.  
Package hyperref Info: Bookmarks ON on input line 4425.  
\c@Hy@tempcnt=\count289  
(c:/TeXLive/2022/texmf-dist/tex/latex/url/url.sty  
\Urlmuskip=\muskip17  
Package: url 2013/09/16 ver 3.4 Verb mode for urls, etc.  
)  
LaTeX Info: Redefining \url on input line 4763.  
\XeTeXLinkMargin=\dimen174  
(c:/TeXLive/2022/texmf-dist/tex/generic/bitset/bitset.sty  
Package: bitset 2019/12/09 v1.3 Handle bit-vector datatype (HO)  
(c:/TeXLive/2022/texmf-dist/tex/generic/bigintcalc/bigintcalc.sty  
Package: bigintcalc 2019/12/15 v1.5 Expandable calculations on big  
integers (HO  
)  
)  
\Fld@menulength=\count290  
\Field@Width=\dimen175  
\Fld@charsize=\dimen176  
Package hyperref Info: Hyper figures OFF on input line 6042.  
Package hyperref Info: Link nesting OFF on input line 6047.  
Package hyperref Info: Hyper index ON on input line 6050.  
Package hyperref Info: backreferencing OFF on input line 6057.  
Package hyperref Info: Link coloring ON on input line 6060.  
Package hyperref Info: Link coloring with OCG OFF on input line 6067.  
Package hyperref Info: PDF/A mode OFF on input line 6072.  
(c:/TeXLive/2022/texmf-dist/tex/latex/base/atbegshi-ltx.sty  
Package: atbegshi-ltx 2021/01/10 v1.0c Emulation of the original atbegshi  
package with kernel methods  
)  
\Hy@abspage=\count291  
\c@Item=\count292  
\c@Hfootnote=\count293  
)  
Package hyperref Info: Driver (autodetected): hpdftex.  
(c:/TeXLive/2022/texmf-dist/tex/latex/hyperref/hpdftex.def  
File: hpdftex.def 2023-02-07 v7.00v Hyperref driver for pdfTeX  
(c:/TeXLive/2022/texmf-dist/tex/latex/base/atveryend-ltx.sty  
Package: atveryend-ltx 2020/08/19 v1.0a Emulation of the original  
atveryend pac  
kage  
with kernel methods  
)  
\Fld@listcount=\count294  
\c@bookmark@seq@number=\count295  
(c:/TeXLive/2022/texmf-dist/tex/latex/rerunfilecheck/rerunfilecheck.sty
```

```
Package: rerunfilecheck 2022-07-10 v1.10 Rerun checks for auxiliary files
(HO)
(c:/TeXLive/2022/texmf-dist/tex/generic/uniquecounter/uniquecounter.sty
Package: uniquecounter 2019/12/15 v1.4 Provide unlimited unique counter
(HO)
)
Package uniquecounter Info: New unique counter `rerunfilecheck' on input
line 2
85.
)
\Hy@SectionHShift=\skip59
) ./cas-common.sty
\l_stm_title_before_dim=\dimen177
\l_stm_title_after_dim=\dimen178
\g_ead_int=\count296
\g_uad_int=\count297
\@eadauthor=\toks26
\g_stm_tnote_int=\count298
\g_stm_fnote_int=\count299
\g_stm_cor_int=\count300
\g_stm_au_int=\count301
\g_stm_aau_int=\count302
\l_autype_int=\count303
\l_stm_augroup_before_dim=\dimen179
\l_stm_augroup_after_dim=\dimen180
\l_stm_augroup_lskip_tl=\dimen181
\l_stm_augroup_rskip_tl=\dimen182
\g_stm_aff_int=\count304
\g_stm_aff_ext_int=\count305
\g_stm_aff_int_int=\count306
\g_stm_fn_aff_ext_int=\count307
\g_stm_fn_aff_int_int=\count308
\l_stm_aff_before_dim=\dimen183
\l_stm_aff_after_dim=\dimen184
\l_stm_aff_lskip_dim=\dimen185
\l_stm_aff_rskip_dim=\dimen186
\g_stm_augr_int=\count309
\g_stm_aaugr_int=\count310
(c:/TeXLive/2022/texmf-dist/tex/latex/moreverb/moreverb.sty
Package: moreverb 2008/06/03 v2.3a 'more' verbatim facilities
(c:/TeXLive/2022/texmf-dist/tex/latex/tools/verbatim.sty
Package: verbatim 2022-07-02 v1.5u LaTeX2e package for verbatim
enhancements
\every@verbatim=\toks27
\verbatim@line=\toks28
\verbatim@in@stream=\read2
)
\tab@position=\count311
\tab@size=\count312
\listing@line=\count313
)
\g_stm_abs_box=\box56
\casgrabsbox=\box57
\casauhlbox=\box58
```

```

\g_stm_key_box=\box59
\g_stm_jtype_int=\count314
\g_stm_blind_int=\count315
\c@au=\count316
\c@cnote=\count317
\c@tnote=\count318
\c@fnote=\count319
\c@aff=\count320
\g_stm_notes_box=\box60
\g_stm_front_box=\box61
\parindent=\dimen187
\subparindent=\dimen188
\FullWidth=\dimen189
\l_tbl_width_dim=\dimen190
\l_tbl_abovecap_skip=\skip60
\l_tbl_belowcap_skip=\skip61
\l_tbl_abovetbl_skip=\skip62
\l_tbl_belowtbl_skip=\skip63
\l_fig_width_dim=\dimen191
\cascaptionbox=\box62
\l_fig_abovecap_skip=\skip64
\l_fig_belowcap_skip=\skip65
\l_fig_abovefig_skip=\skip66
\l_fig_belowfig_skip=\skip67
(c:/TeXLive/2022/texmf-dist/tex/latex/wrapfig/wrapfig.sty
\wrapoverhang=\dimen192
\WF@size=\dimen193
\c@WF@wrappedlines=\count321
\WF@box=\box63
\WF@everypar=\toks29
Package: wrapfig 2003/01/31 v 3.6
)
\l_wrap_figwidth_dim=\dimen194
\l_wrap_fighspace_dim=\dimen195
\l_wrap_figvspace_dim=\dimen196
\l_wrap_fighcorr_dim=\dimen197
\l_wrap_figvcorr_dim=\dimen198
\l_above_bio_dim=\dimen199
\l_wrap_figlcorr_int=\count322
\l_wrap_figlines_int=\count323
\l_bio_text_box=\box64
\c@ca_biology_ctr=\count324
\l_ca_temp_inta=\count325
\leftMargin=\dimen256
\@enLab=\toks30
\@sep=\skip68
\@@sep=\skip69
) (c:/TeXLive/2022/texmf-dist/tex/latex/base/fontenc.sty
Package: fontenc 2021/04/29 v2.0v Standard LaTeX package
) (c:/TeXLive/2022/texmf-dist/tex/latex/stix/stix.sty
Package: stix 2018/04/17 v1.1.3-latex STIX fonts support package
(c:/TeXLive/2022/texmf-dist/tex/latex/base/textcomp.sty
Package: textcomp 2020/02/02 v2.0n Standard LaTeX package
LaTeX Font Info:    Changing ? sub-encoding to TS1/0 on input line 78.

```

```
)  
Now handling font encoding LS1 ...  
... no UTF-8 mapping file for font encoding LS1  
Now handling font encoding LS2 ...  
... no UTF-8 mapping file for font encoding LS2  
LaTeX Font Info: Redeclaring symbol font `letters' on input line 76.  
LaTeX Font Info: Encoding `OML' has changed to `LS1' for symbol font  
(Font) `letters' in the math version `normal' on input line  
76.  
LaTeX Font Info: Overwriting symbol font `letters' in version `normal'  
(Font) OML/cmm/m/it --> LS1/stix/m/it on input line 76.  
LaTeX Font Info: Encoding `OML' has changed to `LS1' for symbol font  
(Font) `letters' in the math version `bold' on input line  
76.  
LaTeX Font Info: Overwriting symbol font `letters' in version `bold'  
(Font) OML/cmm/b/it --> LS1/stix/m/it on input line 76.  
LaTeX Font Info: Redeclaring symbol font `operators' on input line 77.  
LaTeX Font Info: Encoding `OT1' has changed to `LS1' for symbol font  
(Font) `operators' in the math version `normal' on input  
line 77.  
LaTeX Font Info: Overwriting symbol font `operators' in version  
'normal'  
(Font) OT1/cmr/m/n --> LS1/stix/m/n on input line 77.  
LaTeX Font Info: Encoding `OT1' has changed to `LS1' for symbol font  
(Font) `operators' in the math version `bold' on input line  
77.  
LaTeX Font Info: Overwriting symbol font `operators' in version `bold'  
(Font) OT1/cmr/bx/n --> LS1/stix/m/n on input line 77.  
\symbolbold-operators=\mathgroup6  
LaTeX Font Info: Redeclaring symbol font `symbols' on input line 79.  
LaTeX Font Info: Encoding `OMS' has changed to `LS1' for symbol font  
(Font) `symbols' in the math version `normal' on input line  
79.  
LaTeX Font Info: Overwriting symbol font `symbols' in version `normal'  
(Font) OMS/cmsy/m/n --> LS1/stixscr/m/n on input line  
79.  
LaTeX Font Info: Encoding `OMS' has changed to `LS1' for symbol font  
(Font) `symbols' in the math version `bold' on input line  
79.  
LaTeX Font Info: Overwriting symbol font `symbols' in version `bold'  
(Font) OMS/cmsy/b/n --> LS1/stixscr/m/n on input line  
79.  
\symsymbols2=\mathgroup7  
\symsymbols3=\mathgroup8  
\symsymbols4=\mathgroup9  
\symintegrals=\mathgroup10  
LaTeX Font Info: Redeclaring symbol font `largesymbols' on input line  
84.  
LaTeX Font Info: Encoding `OMX' has changed to `LS2' for symbol font  
(Font) `largesymbols' in the math version `normal' on input  
line 8  
4.  
LaTeX Font Info: Overwriting symbol font `largesymbols' in version  
'normal'
```

(Font) OMX/cmex/m/n --> LS2/stixex/m/n on input line 84.
LaTeX Font Info: Encoding `OMX' has changed to `LS2' for symbol font
(Font) `largesymbols' in the math version `bold' on input
line 84.

LaTeX Font Info: Overwriting symbol font `largesymbols' in version
'bold'
(Font) OMX/cmex/m/n --> LS2/stixex/m/n on input line 84.
\symarrows1=\mathgroup11
\symarrows2=\mathgroup12
\symarrows3=\mathgroup13
LaTeX Font Info: Overwriting symbol font `letters' in version `bold'
(Font) LS1/stix/m/it --> LS1/stix/b/it on input line 88.
LaTeX Font Info: Overwriting symbol font `operators' in version `bold'
(Font) LS1/stix/m/n --> LS1/stix/b/n on input line 89.
LaTeX Font Info: Overwriting symbol font `symbols' in version `bold'
(Font) LS1/stixscr/m/n --> LS1/stixscr/b/n on input line
90.
LaTeX Font Info: Overwriting symbol font `symbols2' in version `bold'
(Font) LS1/stixfrak/m/n --> LS1/stixfrak/b/n on input
line 91.

LaTeX Font Info: Overwriting symbol font `symbols3' in version `bold'
(Font) LS1/stixbb/m/n --> LS1/stixbb/b/n on input line
92.
LaTeX Font Info: Overwriting symbol font `symbols4' in version `bold'
(Font) LS1/stixbb/m/it --> LS1/stixbb/b/it on input line
93.
LaTeX Font Info: Overwriting symbol font `integrals' in version `bold'
(Font) LS2/stixcal/m/n --> LS2/stixcal/b/n on input line
94.
LaTeX Font Info: Overwriting symbol font `largesymbols' in version
'bold'
(Font) LS2/stixex/m/n --> LS2/stixex/b/n on input line
95.
LaTeX Font Info: Overwriting symbol font `arrows1' in version `bold'
(Font) LS1/stixsf/m/n --> LS1/stixsf/b/n on input line
96.
LaTeX Font Info: Overwriting symbol font `arrows2' in version `bold'
(Font) LS1/stixsf/m/it --> LS1/stixsf/b/it on input line
97.
LaTeX Font Info: Overwriting symbol font `arrows3' in version `bold'
(Font) LS2/stixtt/m/n --> LS2/stixtt/b/n on input line
98.
LaTeX Font Info: Redeclaring math alphabet \mathit on input line 99.
LaTeX Font Info: Redeclaring math alphabet \mathfrak on input line
102.
LaTeX Font Info: Redeclaring math alphabet \mathsf on input line 106.
LaTeX Font Info: Redeclaring math alphabet \mathtt on input line 108.
LaTeX Font Info: Redeclaring math alphabet \mathbf on input line 109.
LaTeX Info: Redefining \yen on input line 456.
LaTeX Info: Redefining \circledR on input line 458.
LaTeX Info: Redefining \checkmark on input line 460.
LaTeX Info: Redefining \maltese on input line 461.

LaTeX Font Info: Redeclaring math accent \grave on input line 698.
LaTeX Font Info: Redeclaring math accent \acute on input line 699.
LaTeX Font Info: Redeclaring math accent \hat on input line 700.
LaTeX Font Info: Redeclaring math accent \tilde on input line 701.
LaTeX Font Info: Redeclaring math accent \bar on input line 702.
LaTeX Font Info: Redeclaring math accent \breve on input line 703.
LaTeX Font Info: Redeclaring math accent \dot on input line 704.
LaTeX Font Info: Redeclaring math accent \ddot on input line 705.
LaTeX Font Info: Redeclaring math accent \mathring on input line 707.
LaTeX Font Info: Redeclaring math accent \check on input line 708.
LaTeX Font Info: Redeclaring math accent \vec on input line 716.
LaTeX Font Info: Redeclaring math accent \widehat on input line 728.
LaTeX Font Info: Redeclaring math accent \widetilde on input line 729.
LaTeX Info: Redefining \vdots on input line 1518.
LaTeX Info: Redefining \cdots on input line 1522.
LaTeX Font Info: Redeclaring math symbol \mathsterling on input line 1978.
LaTeX Info: Redefining \not on input line 2144.
) (c:/TeXLive/2022/texmf-dist/tex/latex/inconsolata/inconsolata.sty
Package: inconsolata 2019/05/17 v1.12
'inconsolata-z14' v1.12, 2019/05/17 Text macros for Inconsolata (msharpe)
(c:/T
eXLive/2022/texmf-dist/tex/latex/xkeyval/xkeyval.sty
Package: xkeyval 2022/06/16 v2.9 package option processing (HA)
(c:/TeXLive/2022/texmf-dist/tex/generic/xkeyval/xkeyval.tex
(c:/TeXLive/2022/te
xmf-dist/tex/generic/xkeyval/xkvutils.tex
\XKV@toks=\toks31
\XKV@tempa@toks=\toks32
)
\XKV@depth=\count326
File: xkeyval.tex 2014/12/03 v2.7a key=value parser (HA)
)
\zifour@ocount=\count327
) (c:/TeXLive/2022/texmf-dist/tex/latex/geometry/geometry.sty
Package: geometry 2020/01/02 v5.9 Page Geometry
(c:/TeXLive/2022/texmf-dist/tex/generic/iftex/ifvtex.sty
Package: ifvtex 2019/10/25 v1.7 ifvtex legacy package. Use iftex instead.
)
\Gm@cnth=\count328
\Gm@cntv=\count329
\c@Gm@tempcnt=\count330
\Gm@bindingoffset=\dimen257
\Gm@wd@mp=\dimen258
\Gm@odd@mp=\dimen259
\Gm@even@mp=\dimen260
\Gm@layoutwidth=\dimen261
\Gm@layoutheight=\dimen262
\Gm@layouthoffset=\dimen263
\Gm@layoutvoffset=\dimen264
\Gm@dimlist=\toks33
) (c:/TeXLive/2022/texmf-dist/tex/latex/natbib/natbib.sty
Package: natbib 2010/09/13 8.31b (PWD, AO)
\bibhang=\skip70

```
\bibsep=\skip71
LaTeX Info: Redefining \cite on input line 694.
\c@NAT@ctr=\count331
)
LaTeX Font Info: Trying to load font information for T1+stix on input
line 4
4.
(c:/TeXLive/2022/texmf-dist/tex/latex/stix/t1stix.fd
File: t1stix.fd 2015/04/17 v1.1.2-latex STIX T1 font definitions
) (./cas-dc-template.aux)
\openout1 = `cas-dc-template.aux'.

LaTeX Font Info: Checking defaults for OML/cmm/m/it on input line 44.
LaTeX Font Info: ... okay on input line 44.
LaTeX Font Info: Checking defaults for OMS/cmsy/m/n on input line 44.
LaTeX Font Info: ... okay on input line 44.
LaTeX Font Info: Checking defaults for OT1/cmr/m/n on input line 44.
LaTeX Font Info: ... okay on input line 44.
LaTeX Font Info: Checking defaults for T1/cmr/m/n on input line 44.
LaTeX Font Info: ... okay on input line 44.
LaTeX Font Info: Checking defaults for TS1/cmr/m/n on input line 44.
LaTeX Font Info: ... okay on input line 44.
LaTeX Font Info: Checking defaults for OMX/cmex/m/n on input line 44.
LaTeX Font Info: ... okay on input line 44.
LaTeX Font Info: Checking defaults for U/cmr/m/n on input line 44.
LaTeX Font Info: ... okay on input line 44.
LaTeX Font Info: Checking defaults for PD1/pdf/m/n on input line 44.
LaTeX Font Info: ... okay on input line 44.
LaTeX Font Info: Checking defaults for PU/pdf/m/n on input line 44.
LaTeX Font Info: ... okay on input line 44.
LaTeX Font Info: Checking defaults for LS1/stix/m/n on input line 44.
LaTeX Font Info: Trying to load font information for LS1+stix on input
line
4.
(c:/TeXLive/2022/texmf-dist/tex/latex/stix/ls1stix.fd
File: ls1stix.fd 2015/04/17 v1.1.2-latex STIX LS1 font definitions
)
LaTeX Font Info: ... okay on input line 44.
LaTeX Font Info: Checking defaults for LS2/stix/m/n on input line 44.
LaTeX Font Info: Trying to load font information for LS2+stix on input
line
4.
(c:/TeXLive/2022/texmf-dist/tex/latex/stix/ls2stix.fd
File: ls2stix.fd 2015/04/17 v1.1.2-latex STIX LS2 font definitions
)
LaTeX Font Info: ... okay on input line 44.
(c:/TeXLive/2022/texmf-dist/tex/context/base/mkii/supp-pdf.mkii
[Loading MPS to PDF converter (version 2006.09.02).]
\scratchcounter=\count332
\scratchdimen=\dimen265
\scratchbox=\box65
\nofMPsegments=\count333
\nofMParguments=\count334
\everyMPshowfont=\toks34
```

```

\MPscratchCnt=\count335
\MPscratchDim=\dimen266
\MPnumerator=\count336
\makeMPintoPDFobject=\count337
\everyMPtoPDFconversion=\toks35
) (c:/TeXLive/2022/texmf-dist/tex/latex/epstopdf-pkg/epstopdf-base.sty
Package: epstopdf-base 2020-01-24 v2.11 Base part for package epstopdf
(c:/TeXLive/2022/texmf-dist/tex/latex/grfext/grfext.sty
Package: grfext 2019/12/03 v1.3 Manage graphics extensions (HO)
)
Package epstopdf-base Info: Redefining graphics rule for `'.eps' on input
line 4
85.
Package grfext Info: Graphics extension search list:
(grfext)
[.pdf,.png,.jpg,.mps,.jpeg,.jbig2,.jb2,.PDF,.PNG,.JPG,.JPE
G,.JBIG2,.JB2,.eps]
(grfext)                                \AppendGraphicsExtensions on input line 504.
(c:/TeXLive/2022/texmf-dist/tex/latexconfig/epstopdf-sys.cfg
File: epstopdf-sys.cfg 2010/07/13 v1.3 Configuration of (r)epstopdf for
TeX Liv
e
))
LaTeX Info: Command `\'dddot' is already robust on input line 44.
LaTeX Info: Command `\'ddddot' is already robust on input line 44.
Package hyperref Info: Link coloring ON on input line 44.
(./cas-dc-template.out) (./cas-dc-template.out)
\@outlinefile=\write3
\openout3 = `cas-dc-template.out'.

(c:/TeXLive/2022/texmf-dist/tex/latex/upquote/upquote.sty
Package: upquote 2012/04/19 v1.3 upright-quote and grave-accent glyphs in
verba
tim
)
*geometry* driver: auto-detecting
*geometry* detected driver: pdftex
*geometry* verbose mode - [ preamble ] result:
* driver: pdftex
* paper: custom
* layout: <same size as paper>
* layoutoffset:(h,v)=(0.0pt,0.0pt)
* modes:
* h-part:(L,W,R)=(51.4995pt, 494.50888pt, 51.4995pt)
* v-part:(T,H,B)=(55.48286pt, 689.4103pt, 51.784pt)
* \paperwidth=597.50787pt
* \paperheight=796.67715pt
* \textwidth=494.50888pt
* \textheight=689.4103pt
* \oddsidemargin=-20.7705pt
* \evensidemargin=-20.7705pt
* \topmargin=-40.78712pt
* \headheight=12.0pt
* \headsep=12.0pt

```

```
* \topskip=10.0pt
* \footskip=12.0pt
* \marginparwidth=57.0pt
* \marginparsep=11.0pt
* \columnsep=18.0pt
* \skip\footins=9.0pt plus 4.0pt minus 2.0pt
* \hoffset=0.0pt
* \voffset=0.0pt
* \mag=1000
* \@twocolumnfalse
* \@twosidefalse
* \@mparswitchfalse
* \@reversemarginfalse
* (lin=72.27pt=25.4mm, 1cm=28.453pt)
```

! LaTeX Error: The key 'stm/author/<options>' is unknown and is being ignored.

For immediate help type H <return>.

...

1.80 \author[<aff no>]{<author name>} [<options>]

The module 'stm/author' does not have a key called 'stm/author/<options>'.

Check that you have spelled the key name correctly.

! LaTeX Error: The key 'stm/author/<options>' is unknown and is being ignored.

For immediate help type H <return>.

...

1.107 \author[<aff no>]{<author name>} [<options>]

The module 'stm/author' does not have a key called 'stm/author/<options>'.

Check that you have spelled the key name correctly.

```
\verbatim@out=\write4
\openout4 = `cas-dc-template.abs'.
```

Runaway argument?

! Paragraph ended before \verbatim@start was complete.
<to be read again>

\par

1.141

I suspect you've forgotten a `}', causing me to apply this control sequence to too much text. How can we recover?
My plan is to forget the whole thing and hope for the best.

```
LaTeX Font Info:    Trying to load font information for T1+cmss on input
line 2
12.
(c:/TeXLive/2022/texmf-dist/tex/latex/base/t1cmss.fd
File: t1cmss.fd 2022/07/10 v2.51 Standard LaTeX font definitions
)
LaTeX Font Info:    Trying to load font information for LS1+stixscr on
input li
ne 212.
(c:/TeXLive/2022/texmf-dist/tex/latex/stix/ls1stixscr.fd
File: ls1stixscr.fd 2015/04/17 v1.1.2-latex STIX script LS1 font
definitions
)
LaTeX Font Info:    Trying to load font information for LS2+stixex on
input lin
e 212.
(c:/TeXLive/2022/texmf-dist/tex/latex/stix/ls2stixex.fd
File: ls2stixex.fd 2015/04/17 v1.1.2-latex STIX extention LS2 font
definitions

)
LaTeX Font Info:    Trying to load font information for U+msa on input
line 212
.
(c:/TeXLive/2022/texmf-dist/tex/latex/amsfonts/umsa.fd
File: umsa.fd 2013/01/14 v3.01 AMS symbols A
)
LaTeX Font Info:    Trying to load font information for U+msb on input
line 212
.
(c:/TeXLive/2022/texmf-dist/tex/latex/amsfonts/umsb.fd
File: umsb.fd 2013/01/14 v3.01 AMS symbols B
)
LaTeX Font Info:    Trying to load font information for LS1+stixfrak on
input l
ine 212.
(c:/TeXLive/2022/texmf-dist/tex/latex/stix/ls1stixfrak.fd
File: ls1stixfrak.fd 2015/04/17 v1.1.2-latex STIX fraktur LS1 font
definitions
)
LaTeX Font Info:    Trying to load font information for LS1+stixbb on
input lin
e 212.
(c:/TeXLive/2022/texmf-dist/tex/latex/stix/ls1stixbb.fd
File: ls1stixbb.fd 2015/04/17 v1.1.2-latex STIX blackboard LS1 font
definitions

)
LaTeX Font Info:    Trying to load font information for LS2+stixcal on
input li
```

```
ne 212.  
(c:/TeXLive/2022/texmf-dist/tex/latex/stix/ls2stixcal.fd  
File: ls2stixcal.fd 2015/04/17 v1.1.2-latex STIX calligraphic LS2 font  
definitions  
)  
LaTeX Font Info: Trying to load font information for LS1+stixsf on  
input line 212.  
(c:/TeXLive/2022/texmf-dist/tex/latex/stix/ls1stixsf.fd  
File: ls1stixsf.fd 2015/04/17 v1.1.2-latex STIX sans-serif LS1 font  
definitions  
)  
LaTeX Font Info: Trying to load font information for LS2+stixtt on  
input line 212.  
(c:/TeXLive/2022/texmf-dist/tex/latex/stix/ls2stixtt.fd  
File: ls2stixtt.fd 2015/04/17 v1.1.2-latex STIX typewriter LS2 font  
definitions  
) [1{c:/TeXLive/2022/texmf-var/fonts/map/pdftex/updmap/pdftex.map}  
])  
! Emergency stop.  
<*> cas-dc-template.tex  
  
*** (job aborted, no legal \end found)
```

Here is how much of TeX's memory you used:

```
16763 strings out of 476024  
253858 string characters out of 5794017  
1860382 words of memory out of 5000000  
36933 multiletter control sequences out of 15000+600000  
543431 words of font info for 80 fonts, out of 8000000 for 9000  
1141 hyphenation exceptions out of 8191  
90i, 9n, 93p, 282b, 513s stack positions out of  
10000i, 1000n, 2000p, 200000b, 200000s  
! ==> Fatal error occurred, no output PDF file produced!
```

```
% Copyright 2019-2021 Elsevier Ltd
%
% This file is part of the 'CAS Bundle'.
%
-----
%
% It may be distributed and/or modified under the
% conditions of the LaTeX Project Public License, either version 1.2
% of this license or (at your option) any later version.
% The latest version of this license is in
%   http://www.latex-project.org/lppl.txt
% and version 1.2 or later is part of all distributions of LaTeX
% version 1999/12/01 or later.
%
% The list of all files belonging to the LaTeX 'CAS Bundle' is
% given in the file `manifest.txt'.
%
% CONTENTS OF THE CAS BUNDLE
=====
```

Directory elsevier-cas-template/

cas-sc.cls
Classfile to be used for single column format

cas-dc.cls
Classfile to be used for double column format

cas-model2-names.bst
BibTeX style file

cas-sc-template.tex
TeX template

cas-dc-template.tex
TeX template

manifest.txt
this file

README
small readme documentation

Directory doc/

The following files are graphic files needed for creating pdf output
of the documentation from elsdoc.tex:

dc-sample.pdf
sc-sample.pdf

elsdoc-cas.tex -- LaTeX source file of documentation
elsdoc-cas.pdf -- documentation for elsarticle.cls

Directory thumbnails/

Contains thumbnail images which will be included in the typeset PDF.

```
cas-email.jpeg  
cas-facebook.jpeg  
cas-gplus.jpeg  
cas-linkedin.jpeg  
cas-twitter.jpeg  
cas-url.jpeg
```

The following files are written out every time `elsdoc.tex` is compiled:

```
elsdoc-cas.aux  
elsdoc-cas.log  
elsdoc-cas.out  
tmp-cas.tex
```

Auxiliary packages needed to generate pdf output from `elsdoc.tex`:

```
rvdtx.sty  
pdfwidgets.sty  
glyptounicode.tex
```



Click here to access/download
LaTeX Source File
cas-sc-template.abs



Click here to access/download
LaTeX Source File
cas-sc-template.blg



Click here to access/download
LaTeX Source File
README



Click here to access/download
LaTeX Source File
cas-sc-template.aux



Click here to access/download
LaTeX Source File
cas-sc-template.log



Click here to access/download

LaTeX Source File

[**3fe827d8-1d09-4efc-a76a-9245a31dbf44**](#)



Declaration of interests

The authors declare that they have no known competing financial interests or personal relationships that could have appeared to influence the work reported in this paper.

The authors declare the following financial interests/personal relationships which may be considered as potential competing interests: